JPL Publication 19-10

Mars Exploration Rover *Opportunity* End of Mission Report

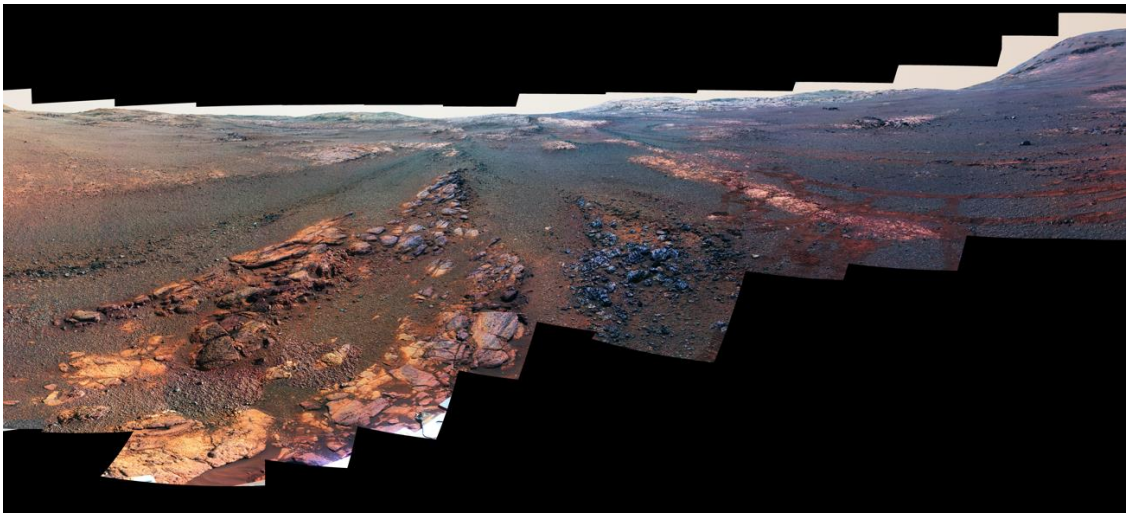

John L. Callas, Project Manager
Matthew P. Golombek, Project Scientist
Abigail A. Fraeman, Deputy Project Scientist
Mars Exploration Rover Project
Jet Propulsion Laboratory, California Institute of Technology

National Aeronautics and Space Administration

Jet Propulsion Laboratory
California Institute of Technology
Pasadena, California

October 2019

This research was carried out at the Jet Propulsion Laboratory, California Institute of Technology, under a contract with the National Aeronautics and Space Administration.

Contents

1 Abstract

The Mars Exploration Rover (MER) *Opportunity* landed on Meridiani Planum on 25 January 2004 for a prime mission designed to last three months (90 sols). After more than fourteen years operating on the surface of Mars, the last communication from *Opportunity* occurred on sol 5111 (10 June, 2018) when a major dust storm reduced power on the solar panels to the point where further communications were not possible. Following the cessation of the dust storm several weeks later, the MER project radiated over 1000 commands to Mars in an attempt to elicit a response from the rover. Attempts were made utilizing the Deep Space Network X-Band and UHF relay via both Mars Odyssey and the Mars Reconnaissance Orbiter. Search and recovery efforts concluded on 12 February, 2019. It is the MER project's assessment that the environmental window in which it would be most probable to recover *Opportunity* had passed by that time and that the rover would succumb to the extreme environmental conditions experienced during a winter on Mars. This report summarizes the major science accomplishments throughout the fourteen years of this mission, with a detailed focused on recent science accomplishments during the last extended mission (EM-11). This report also describes the mission engineering accomplishments and specific actions taken during the attempt to recover the vehicle after communications were lost during the major dust storm.

2 Summary of major science accomplishments of the mission

The Mars Exploration Rover (MER) *Opportunity* landed on Meridiani Planum on January 25, 2004 and maintained communications with Earth until June 10, 2018, when a major dust storm reduced power on the solar panels to the point where further communications were not possible. *Opportunity* far exceeded its 90-sol primary mission and set records for longevity (5111 sols), distance traveled (~45 km, Fig. 2.1), and scientific discoveries for planetary rovers. This section highlights the scientific legacy derived from analysis of imaging and spectroscopic data acquired using *Opportunity's* instrument payload (Squyres et al., 2003).

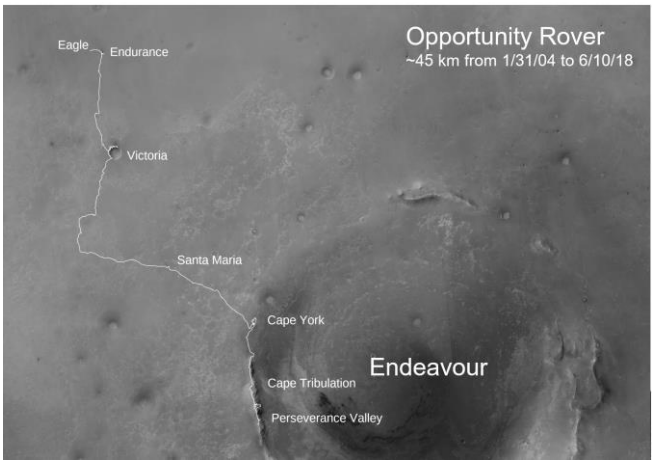

Fig. 2.1: HiRISE image mosaic showing the complete traverse of *Opportunity* across Meridiani Planum and onto Endeavour Crater's (22 km diameter) western rim segments. Names on the plains refer to craters examined by *Opportunity* to characterize Burns formation sulfate-bearing strata. Erebus Crater, not shown, is just north of Victoria Crater.

Opportunity was the first landed mission to identify and characterize a sedimentary rock record on a planetary body other than Earth. The Burns formation, named in honor of Roger Burns, is a >> 10s of meters thick section of genetically related sedimentary rock that outcrops in the walls of craters and regional fractures throughout Meridiani Planum (Grotzinger et al., 2006). *Opportunity* documented the primary sedimentary features (e.g., bedding, grain size distributions) and

diagenetic features of the Burns formation to determine ancient environmental conditions (Fig. 2.2). *Opportunity* data showed Fe-, Mg-, and Ca sulfates were present in the Burns formation, the first instance these minerals were detected on Mars. The presence of sulfate salts combined with sedimentary structure analyses supported a model of saline groundwaters ascending through the Noachian basement to produce evaporitic sulfate-rich muds in an interdune environment (Squyres & Knoll, 2005; Hurowitz et al., 2010; among many!). Reworking by wind and water generated the "second-cycle" sulfate-cemented, cross-bedded Burns formation sandstones that underlie Meridiani Planum (Grotzinger et al., 2006; McLennan et al. 2005). *Opportunity* also discovered hematite concretions ("blueberries") weathering out of Burns formation rocks, another first for a landed Mars missions. The presence of concretions both confirmed the orbital detection of hematite that lead to the selection of Meridiani Planum as a landing site (Christensen et al., 2001) and it provided evidenced later periods of rising ground waters (McLennan et al., 2005). In summary, the first sedimentary deposit characterized on another planet by *Opportunity* demonstrated the prolonged presence of water on and beneath the surface of Mars.

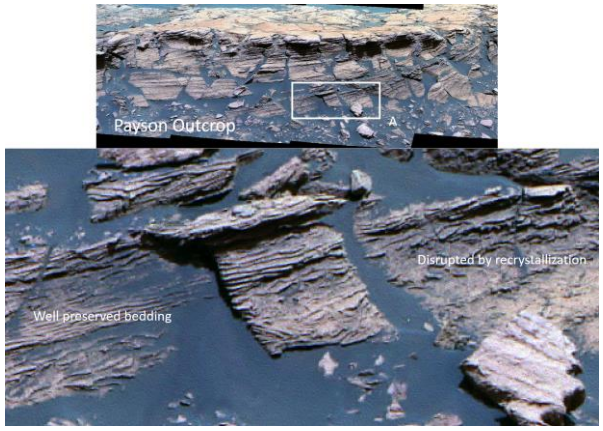

Fig. 2.2: View of the Payson outcrop on the western side of Erebus crater. This outcrop displays evidence for interdune wet conditions, including the presence of shallow surface water flow based on ripple patterns. There is also evidence for bedding disruption by recrystallization soon after deposition of the sulfate-rich deposits.

Opportunity reached the western rim of Endeavour crater in December 2010, nearly seven years into its mission. Endeavour crater is a ~22 km diameter impact crater that predates the deposition of the Burns formation (Arvidson et al., 2006). The rocks that compose Endeavour's rim are Noachian in age and are the oldest rocks ever visited by a landed mission anywhere on Mars. *Opportunity*'s investigation of the area provide insight into the environmental conditions during that epoch of Mars' history.

Opportunity data show that Endeavour's rim is composed of coarse impact breccias (designated the upper Shoemaker formation) that overlie a pre-impact substrate that includes lower Shoemaker formation breccias and the pre-impact Matijevic formation (Fig. 2.3) (Mittlefehldt et al., 2019). *Opportunity* found evidence all of these rocks were altered by water, some in benign environments that could have been habitable for microbial life.

The Matijevic formation is the oldest and rarest of the Endeavour rim rocks, and is composed of bright, fine-grained sedimentary rocks (Arvidson et al., 2014; Crumpler et al., 2015). The original depositional setting of the Matijevic formation is enigmatic due to the unit's limited spatial extent and lack of geologic context, but high Ni and low MgO compositions suggest it was altered by water either pre-Endeavour or post-Endeavour impact (Mittlefehdlt et al., 2018).

The Shoemaker formation overlies the Matijevic formation and is composed of impact breccias with sub rounded-to-angular centimeter-scale clasts (Arvidson et al., 2014; Crumpler et al., 2015; Squyres et al., 2012). It is the most commonly observed rock type on Endeavour's rim

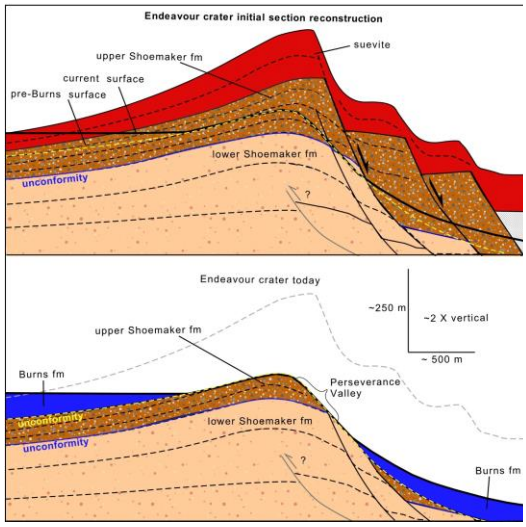

Fig. 2.3: Schematic cross sections showing the original and partially eroded versions of the structure and geology inferred for Endeavour's rim.

and has chemical evidence for multiple episodes and styles of aqueous alteration (low temperature, high temperature, low pH, neutral pH) (Squyres et al., 2012; Mittlefehldt et al., 2018).

The Compact Reconnaissance Imaging Spectrometer for Mars (CRISM) showed Fe/Mg phyllosilicates were present in the rim of Endeavour crater (Wray et al., 2009). Fe/Mg phyllosilicates are some of the most commonly detected alteration minerals from visible orbital spectral datasets, and *Opportunity* was the first rover to examine the geologic setting of these detections from the ground. At Cape York, *Opportunity* found Matijevic formation rocks were covered by dark veneers that were enriched in volatile/mobile elements and which were thought to be the source of Fe/Mg phyllosilicate CRISM signatures in that area (Arvidson et al., 2014; Clark et al., 2016; Crumpler et al., 2015). Cross-cutting relationship showed the veneers formed post-impact (Mittlefehldt et al., 2018). At Marathon Valley, *Opportunity* found isochemical alteration caused by small amounts of circumneutral pH water along fractures in the Shoemaker formation that formed ferric-bearing phyllosilicates (Fox et al., 2016).

Evidence for aqueous alteration concentrated along fractures was common in Endeavour, highlighting a dominance by ground water related processes. *Opportunity* was the first rover to discover gypsum veins on Mars, indicating low-temperature (<50˚ C) fluid through some fractures in Endeavour's rim. *Opportunity* also found rare decimeter-scale boxwork fractures that contained Al-rich phyllosilicates, which reflect an episode of extensive leaching under higher temperatures (Arvidson et al., 2014; Clark et al., 2016). Finally, the rover wheels serendipitously upturned two unique rocks named Pinnacle Island and Stuart Island that had high Mn and S contents indicating an evaporative aqueous environment followed by alteration with a strong oxidant(s) that precipitated Mn oxide(s) intermixed with sulfate-rich salt coatings (Arvidson et al., 2016).

Opportunity's extensive exploration of Endeavour crater's western rim segments (Fig. 2.1) also provided the first detailed view of the rim a complex crater on any planet (Crumpler et al., 2019). Impact cratering is a ubiquitous geologic process throughout the entire solar system, and *Opportunity's* mapping has broad reaching implications in planetary science, in addition to insight they provide into Mars' history. One unexpected characteristic of Endeavour's rim is that it is segmented into topographically and structurally distinct domains bounded by radial fractures located both within and between segments. Abrupt along-strike termination of outcrops, right and left-stepping offsets of local topographic rim crests, and changes in strike and dip of local slabs and foliations are evident at the transitions between rim segments. Inner crater rim units dip toward the crater interior and are interpreted to be due to uplift over blind thrust faults generated at the time of crater formation. Fluvial erosion of Endeavour, followed by minor weathering,

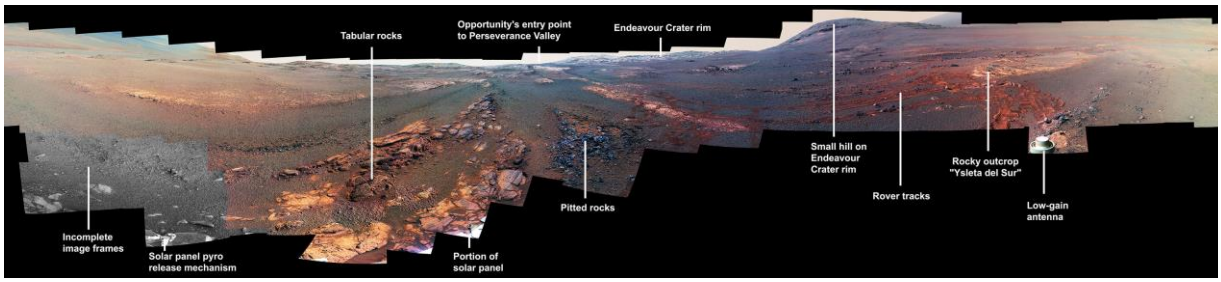

Fig. 2.4: Pancam-based view from *Opportunity* looking uphill toward the top of Perseverance Valley, showing what are interpreted to be various outcrops juxtaposed by faulting and shaped by wind action.

mass movements, and wind action, are interpreted to have produced the current shape and rock exposures characterized by *Opportunity* (Grant et al. 2016, Hughes et al., 2019).

Opportunity ended its mission characterizing Perseverance Valley, a distinct geomorphic feature in the rim of Endeavour crater in orbital images. Hypotheses for Perseverance Valley's formation were that is was a fluvial or debris flow feature. *Opportunity* data from the upper 2/5 of the valley (all that could be explored before the dust storm) do not resolve the formation mechanism, but they did inspire three additional hypotheses that the valley could results from wind erosion of a complex fault system, fault reactivation and eolian erosion, or dry boulder falls (Arvidson et al., 2019; Sullivan et al., 2019; Beer et al., 2019) (Fig. 2.4).

Opportunity was the first planetary rover to identify and characterize meteorites. Analyses of the extent of meteorite weathering in Meridiani was used to characterize the post-Burns formation atmosphere-surface physical and chemical processes and rates (Ashley et al., 2015; Chappelow and Golombek, 2011 JGR, Schröder et al., 2016).

Observations of craters along *Opportunity's* traverse have shown that saltating basaltic sand rapidly erodes craters (Grant et al., 2006; Golombek et al., 2006), and have provided insight into how these craters have degraded through time (Grant et al., 2006; 2008; 2016). In addition, ~100 small craters visited by *Opportunity* have been used to constrain the age (50–200 ka) of the latest phase of ripple migration (Golombek et al., 2010) and to develop a timescale of crater modification over the past 20 Ma based on their degradation state (Golombek et al., 2014). This work has spurred key research into the links between eolian activity and climate (e.g., Golombek et al., 2014, Fenton et al., 2018).

Opportunity provided a legacy of the longest record of *in situ* atmospheric measurements of any *in situ* mission, including aerosol opacities (tau) and characteristics (Lemmon et al, 2015), continued search for dust devils, and aphelion water ice clouds. *Opportunity* observed eight dust events. A twenty-frame thumbnail mosaic acquired on sol 4975 (L_s=118˚ southern winter season) showed the presence of what are likely water ice clouds. These measurements and discoveries form a part of a time series used in determining inter-annual atmospheric processes and dynamics.

The biggest atmospheric event *Opportunity* observed was the development of the largest planet encircling dust event since surface observations began with the two Viking Landers in 1976. The atmospheric normal optical depth measured by Pancam on 6/10/18 (sol 5111, L_s=196,

southern spring season) was at least 10.8, equivalent to a loss of solar radiance on the solar panels of a factor of ~44 relative to more normal opacities. Communication with *Opportunity* was lost the next sol.

The abundance of argon in the Martian atmosphere was measured directly by *Opportunity*'s APXS, with over 2,200 hours of atmospheric spectra acquired to date. Non-condensable gases, e.g., argon, accumulate over the winter poles as CO_2 ice accumulates. As the ice sublimates during the ensuing spring seasons a global CO_2 pressure gradient pushes the argon-enriched air to lower latitudes. *Opportunity*'s measurements of argon have provided an effective method for monitoring these atmospheric dynamics and condensation flows as a function of season and on an inter-annual basis. At low latitudes *Opportunity's* APXS is even more sensitive to detection of argon than Odyssey's GRS (e.g. Sprague et al., 2012). Analyses of APXS atmospheric spectra uncovered a repeated short-term argon enrichment (~L_s 155˚) that is superimposed on the long-period annual variation (Figure 2.5) (Van Bommel et al., 2018). Observations with *Opportunity's* APXS thus represent the first detection of a short-term enrichment of non-condensable gases in the equatorial region of Mars.

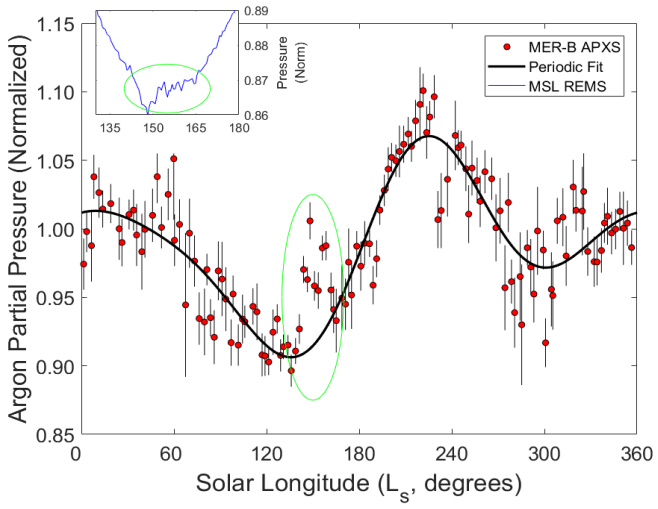

Fig. 2.5: *Opportunity* APXS argon data fit with a sinusoidal trend showing low concentrations during formation of the southern winter cap. The deviation around Ls 155 (highlighted in green) is consistent with a northward migrating front enriched in noncondensable gases. A more-subtle southward migrating front is evident ~Ls 335.

3 Detailed recent science accomplishments

Opportunity spent its last extended missions (EM-10 and 11) exploring and characterizing the rim of Endeavour crater, and high-level scientific findings from EM-10 and 11 are summarized below.

3.1 Testing Hypotheses for the Origin and Evolution of Perseverance Valley

The centerpiece of *Opportunity* EM-10 and EM-11 proposals was the exploration and characterization of Perseverance Valley, a ~200 m long, ~10 to 20 m wide anastomosing set of shallow, channel-like features extending down Endeavour's inner rim from a gentle swale between Capes Tribulation and Byron (Fig. 3.1). *Opportunity* traversed ~40% of the way down Perseverance Valley and conducted numerous imaging and compositional measurements with the goal to determine the geologic process(es) that formed the valley.

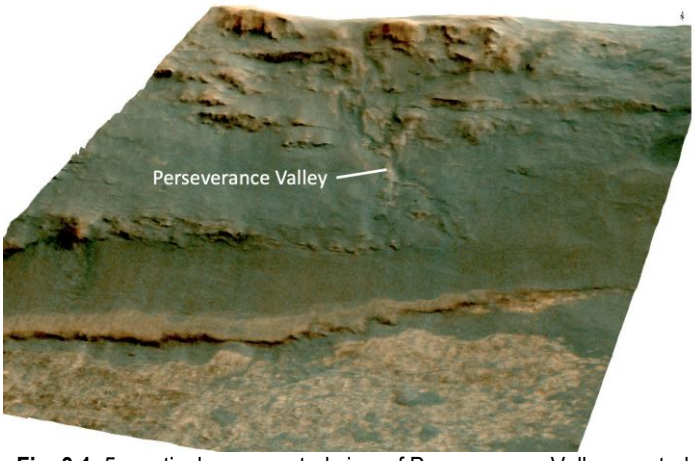

Fig. 3.1: 5x vertical exaggerated view of Perseverance Valley created from HiRISE image EPS_036753_1775 and associated digital elevation model.

While most of Perseverance Valley was left unexplored and definitive evidence for a unique origin still lacking, there are inferences about its origin that can be made with data in hand. Within Perseverance Valley, *Opportunity* found rocks with different textures and compositions juxtaposed against one another. These rocks were aligned roughly perpendicular to Endeavour's rim, consistent with a radial fracture system (e.g., Fig. 2.4). Perseverance Valley may represent a fracture system that was easily eroded relative to more coherent bedrock.

Wind may have been an erosional agent that carved the valley. Clear evidence for wind erosion was found in several outcrops, including miniature sculpted wind tails pointing uphill (Fig. 3.2) (Sullivan et al., 2018). An easterly (up-valley) wind direction is also consistent with what has been inferred from megaripples on Meridiani Planum (Arvidson et al., 2011), the presence of yardang-like features tens of meters long on Cape Dromedary to the south of Cape Byron and on the eastern rim segments (Hughes et al., 2019), and theoretical mesoscale atmospheric circulation models for various Milankovitch cycles (Fenton et al., 2018). Finally, a topographic profile from the entrance of Perseverance Valley downhill, past the Grasberg and Burns formation outcrops located inside Endeavour, is smooth and graded, consistent with continued easterlies that have excavated the interior deposits and the fractures that dominate Perseverance Valley (Hughes et al., 2019). Thus one hypothesis for the valley's origin supported by data collected by *Opportunity* is that it is a deep seated fault system has in full or in part been differentially eroded to form an anastomosing channel-like system.

A second hypothesis is reactivations along the fracture/fault planes since the Noachian that renew relief against ongoing eolian abrasion (Sullivan et al., 2019). Examples of minor fault/fracture activation occurring on relatively recent timescales comparable with eolian

abrasion and ripple migration were observed elsewhere along the rover's long traverse (Sullivan et al., 2018). Fracture/faulting concepts are challenged to explain the location of Perseverance Valley subjacent to a low area along Endeavour's rim. One suggestion under evaluation is that a low area between higher rim segments to either side could be a logical place for stress-adjusting fault reactivations to be focused as a response to the higher rim segments on either side unloading mass at different rates over a long erosional history (Sullivan et al., 2018; 2019).

A third hypothesis is Perseverance valley formed by rockfall-driven bedrock erosion (Beer et al., 2019). Rockfall-driven bedrock erosion is a little recognized actor of rocky slope erosion and channelization, and a potential sustainer of the rugged topography during degradation of crater walls. Laboratory experiments and theoretically modeling show that erosive boulder transport over shallow-angled bedrock slopes similar to the 10-20˚ slopes of Endeavour crater is possible. More erodible bedrock and focused rockfall sources allow topographic steering of boulders to create self-formed channels, even in the absence of a fluid. The rugged cliffs and chutes on the walls of Endeavour crater are potentially shaped and maintained by this process (Beer et al., 2019).

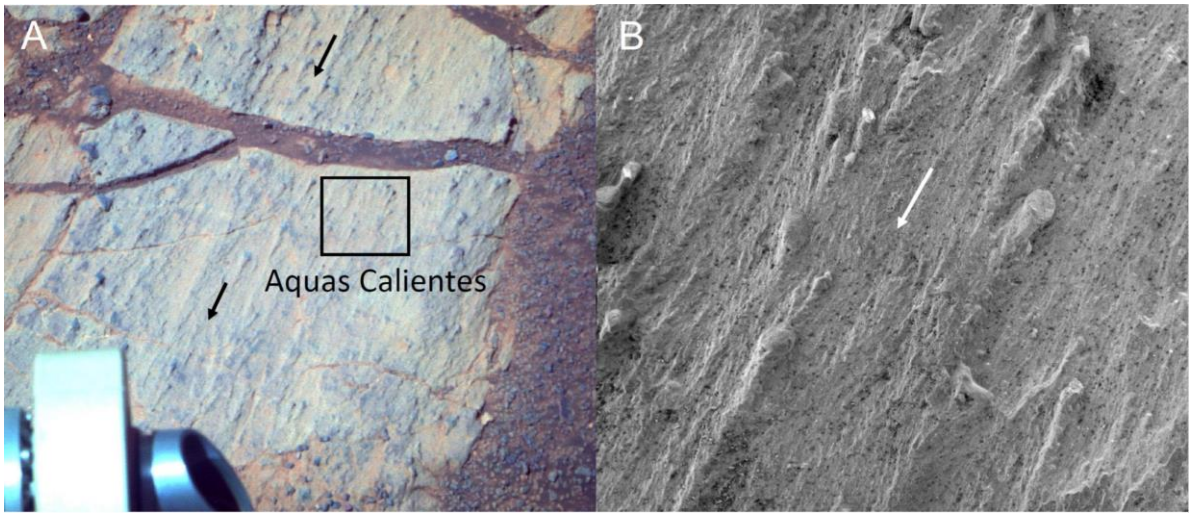

Fig. 3.2: Wind tails pointed uphill inside Perseverance Valley

3.2 Degradation Exposes Structural and Stratigraphic Complexities on Endeavour's Rim

As previously mentioned, *Opportunity's* exploration of Endeavour's rim provided a unique set of measurements about the structure of impact craters. Craters the size of Endeavour are not well-preserved on Earth (e.g., French, 1998; Grieve and Therriault, 2004), and no other Martian rover has been able to traverse and make detailed measurements on the rim of a large (>20 km) Noachian-age impact crater. *Opportunity*'s exploration of Endeavour's rim combined with extensive observations from the Mars Express and Mars Reconnaissance Orbiters provided unique and quantitative insights into the processes that have degraded this 22 km wide Noachian age impact crater. Endeavour crater has undergone a significant amount of erosion relative to the nearby, more youthful Bopolu crater. Landscape evolution models using both datasets indicate that after an early period of fluvial action only Endeavour's tectonic (i.e., outer) rim remained and ~0.5 km of fluvial-deltaic-lacustrine sediment was deposited on the crater floor (Grant et al.,

2016; Hughes et al., 2019). Simulations also show pediments formed on Endeavour's external rim segments during this period, likely as part of a fluvial piedmont system of upland rocks, pediment surfaces, and distal alluvial fans. Orbital and rover-based observations also show that Late Noachian to Early Hesperian age Grasberg formation clastic rocks and Burns formation sulfate-rich sandstones subsequently buried all but high standing Endeavour tectonic rim segments (Fig. 2.3).

The extensive erosion of Endeavour's rim allowed *Opportunity* to characterize in detail the structural, stratigraphic, textural, and compositional nature of tectonic rim rocks, as opposed to overlying largely unconsolidated ejecta deposits. Endeavour's rim is segmented into topographically and structurally distinct domains bounded by radial fractures located both within and between segments (Crumpler et al., 2017). The rim segments vary between 200 m and 300 m wide, with relief from a few tens of meters to 150 m above the surrounding exterior plains (Crumpler et al., 2015) (Fig. 3.3). Geologic and structural mapping using *Opportunity's* observations suggest divisions between rim segments are vertical fracture zones and faults. The faults strike radially across the crater rim, and deformation between segments may be the result of scissor faults separating blocks that experienced differing magnitudes of uplift during crater formation (Crumpler et al., 2018). Differential uplift is consistent with upward and radial compression of the upper crust during crater formation by discontinuous oblique thrust faults along discrete blocks. The relative motion between blocks required accommodation by vertical dip, oblique slip scissor faulting, a process noted in the rim of Meteor crater (Sharpton, 2014; Shoemaker and Kieffer, 1974) and other more deeply eroded craters where faults are exposed (Kenkmann et al., 2014).

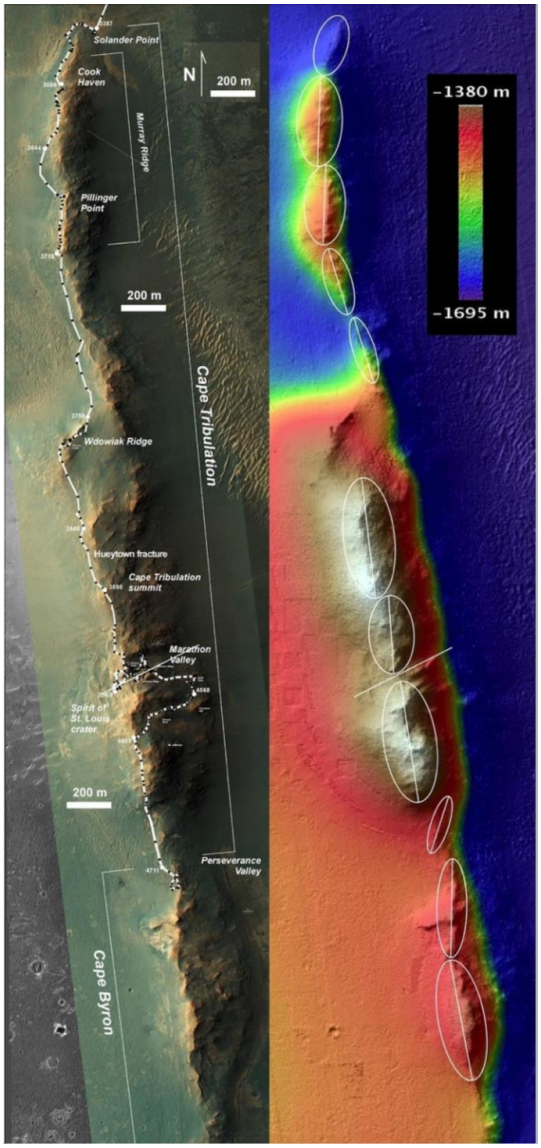

Fig. 3.3: HiRISE (left) and DEM (right) image showing structurally distinct rim segments of the western edge of Endeavour crater.

A second result of in situ mapping is the discovery that the attitudes of foliations and planar contacts between stratigraphic units drape antiformally across the rim, i.e inward toward the center of the crater, as well as outward toward the surrounding plains (Crumpler et al., 2018). Mapping of the attitudes of the contacts and pervasive foliations in outcrops at several locations shows that the inner crater rim units dip inward toward the crater interior. Although inward dips

are unanticipated, they are not excluded by existing models of complex impact craters that otherwise assume monotonically outward-dipping structure. Deep monoclinal structures beneath the tectonic rims of deeply eroded terrestrial impact structures have been documented (Kenkmann et al., 2014). Working hypotheses for observed monoclinal inward-dips along the rim of Endeavour include uplift over blind thrust faults proposed to occur at the time of crater formation (Sharpton, 2014; Kenkmann et al., 2014). This results in asymmetric antiformal crustal deformation, drag folding of uplifted and ejecta-thickened rims during post-impact tectonic-scale slumping of the rim and walls after crater formation, cantilevering of the resistant rim outcrops into the crater during much later degradation, and back wasting of the inner crater walls, or a combination of these processes.

Based on the results of in situ mapping by *Opportunity*, a new, detailed model of crater rim structure is emerging (Fig. 2.3) that gives context for understanding the state of erosion and structural influences on geological and geochemical characteristics observed at outcrops along the crater rim.

4 Mission success score card

The table below shows how *Opportunity* (MER-B) and twin rover Spirit (MER-A) not only achieved but far surpassed all original mission success criteria.

Mission Success Criteria	MER-A Status	MER-B Status	Minimum Mission Success Achieved?		Full Mission Success Achieved?	
# Sols of Operation	2210	5111	√	(1x90 t=0.5)	√	(2x90 t=0.5)
# Sols of simultaneous operation	N/A	2190	N/A		√	(30)
Athena Payload Operation	-	-	√	Both MERs, Pancam + one other	√	Both MERs, full Athena
Pancam observations	thousands	thousands	N/A		N/A	
Mini-TES observations	hundreds	hundreds	N/A		N/A	
MI observations	thousands	thousands	N/A		N/A	
MB observations	hundreds	hundreds	N/A		N/A	
APXS observations	hundreds	hundreds	N/A		N/A	
360 deg color panorama	hundreds	hundreds	√	(One MER)	√	(Both MERs)
360 deg Stereo panorama	hundreds	hundreds	√	(One MER)	√	(Both MERs)
Freshly exposed rocks (RAT)	dozens	dozens	N/A		√	(1)
Image of freshly exposed rock	dozens	dozens	N/A		√	(1)
Complementary analysis of freshly exposed rock	dozens	dozens	N/A		√	(1)
# Locations Investigated	hundreds	hundreds	√	(4)	√	(8)
Drive distance (m)	7730	45161	√	(300)	√	(600)

5 Rover statistics

Detailed statistics documenting actuator usage, drives, instrument deployment device (IDD) use, and data volume returned, number of images acquired, power switch actuations, and other miscellaneous topics over the course of *Opportunity's* entire mission are presented in the following sections.

5.1 Actuator Usage

Mobility Actuator	Motor Revs (M)
Left Front Wheel	92.717
Left Middle Wheel	89.107
Left Rear Wheel	91.216
Right Front Wheel	92.431
Right Middle Wheel	88.873
Right Rear Wheel	90.975
Left Front Steering	4.284
Left Rear Steering	3.489
Right Front Steering (1)	0.356
Right Rear Steering	3.502

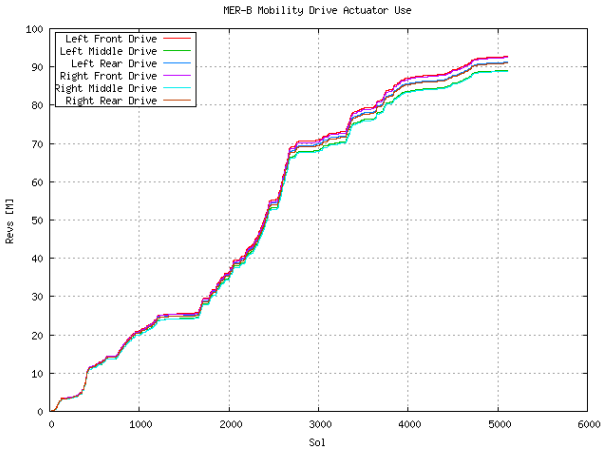

PMA Actuator	Motor Revs (M)
PMA Azimuth	104.271
PMA Camera Elevation	13.896
PMA MTES Mirror El.	1.448

HGA Actuator	Motor Revs (M)
HGA Azimuth	6.343
HGA Elevation	9.317

RAT Actuator (2)	Motor Revs (M)
RAT Revolve	3.960
RAT Grind	36.328

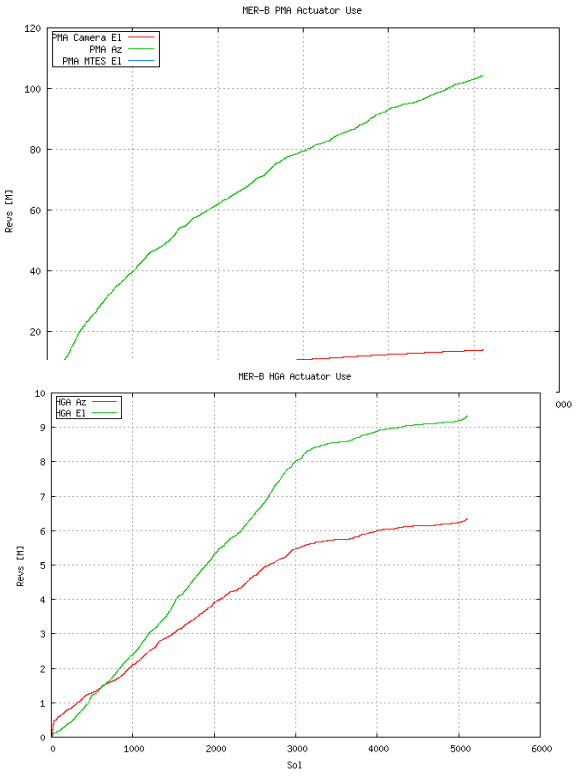

RAT Actuator (2)	Distance (M)
RAT Z Axis	3.437

IDD Actuator (3)	Motor Revs (M)
IDD Shoulder Azimuth	2.385
IDD Shoulder Elevation	3.994
IDD Elbow	6.102
IDD Wrist	1.022
IDD Turret	2.282

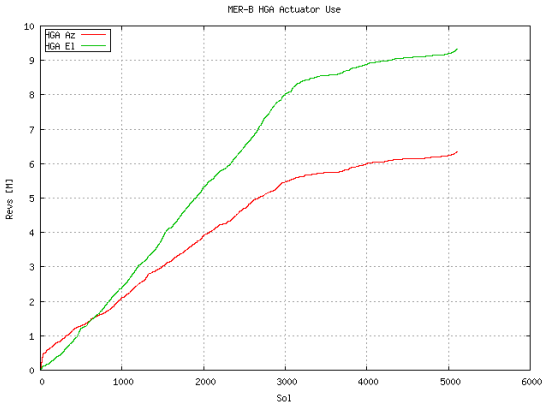

PMA Filter Wheel Actuators (4)	Motor Revs (K)
PMA Left Filter Wheel	24.416
PMA Right Filter Wheel	18.339

MI Dust Cover Actuator (4)	Actuations (4)
MI Dust Cover	1630

Actuator Usage Notes:

1. The Right Front Steering actuator jammed on Sol 433.
2. The RAT Revolve and Grind encoders were lost on Sol 1045 and the RAT Z Axis encoder was lost on Sol 1759. Revolutions since then have been estimated from usage time and/or measured travel distance.
3. The IDD Shoulder Azimuth actuator degraded on Sol 654, degraded further and was declared failed on Sol 1502.
4. The Filter Wheel and MI Dust Cover actuators are stepper motors, the rest are brushed motors. A Dust Cover actuation is an open operation or a close operation.
5. Brushed motors were stress tested to 2 M revs to simulate a 10 M rev lifetime. Expected prime mission lifetime was 2.5 M revs.

5.2 Drive Statistics

Drive Type	Sols
Bumps (drive < 5 m)	363
Drives	1040
Total	1403

Min. Annual Odometry	85.03 m
Max. Annual Odometry	7,855.73 m

Longest Drives	Sol
219.89 m	410
190.28 m	408
183.04 m	406
177.51 m	383

Year	Cumulative Odometry	Annual Odometry
2004	2,051.03 m	2,051.03 m
2005	6,502.15 m	4,451.12 m
2006	9,792.99 m	3,290.84 m
2007	11,591.21 m	1,798.22 m
2008	13,617.33 m	2,026.12 m
2009	18,927.56 m	5,310.23 m
2010	26,505.64 m	7,578.08 m
2011	34,361.37 m	7,855.73 m
2012	35,438.37 m	1,077.00 m
2013	38,729.91 m	3,291.54 m
2014	41,567.25 m	2,837.34 m
2015	42,647.09 m	1,079.84 m
2016	43,733.77 m	1,086.68 m
2017	45,076.01 m	1,342.24 m
2018	45,161.04 m	85.03 m

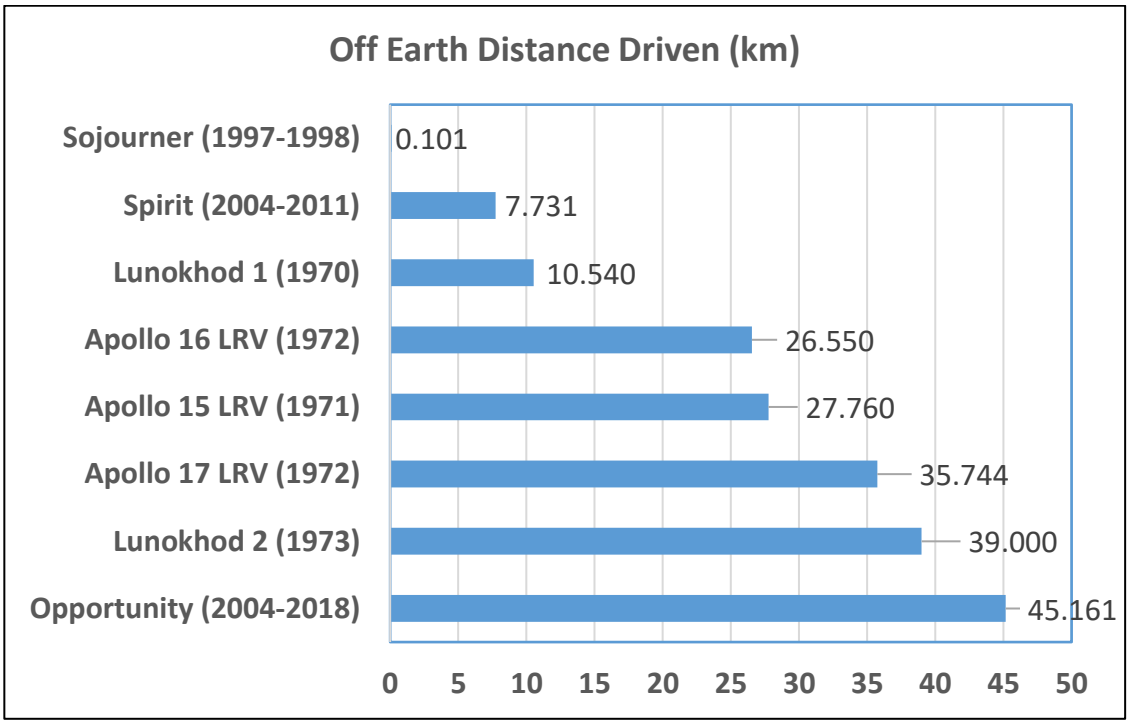

Opportunity passed a marathon (42.195 km) on Sol 3968.

5.3 IDD Statistics

IDD Sols	1495

IDD Tool Use	**Sols**
Mossbauer Spectrometer	489
Alpha Particle X-Ray Spectrometer	988
Microscopic Imager	699
Rock Abrasion Tool (RAT)	70

RAT Brushes	72
RAT Grinds	52

Mini-Thermal Emission Spectrometer	1083 Sols

5.4 Telecom Statistics

Telecomm Usage	**Hours**	**Cycles**
SSPA-A (X-band TX) Power	691.8	4511
CE-505 (UHF) Power	1172.3	5129

Telecom Switch Actuations	**Actuations**
WTS	8435
Coax 0	0
Coax 1	45
Coax 2	2

Data Return	**Number of Passes**	**Percent of Passes**	**GBytes Received**	**Percent of Data Return**
MGS	82	1.4	0.39	0.9
ODY	4594	78.8	38.58	91.9
MRO	551	9.5	2.54	6.0
DTE	588	10.1	0.45	1.1
MEX	15	0.03	0.01	0.0
Total	5830	--	41.96	--

5.5 Imaging Statistics

Images by camera	Number
EDL	3
Front Hazcam	12,733
Rear Hazcam	5,945
MI	11,606
Navcam	48,390
Pancam	13,8917
Total	217,594

Avg. Images/Sol	42.574	(5111 Sols)
Avg. Images/km	4,818.2	(45.1610 km)
Avg. Images/year	15,135.4	(14.3765 yr)

Total Camera On-Time	4,739.0 hr
Camera Power Cycles	16,139

5.6 Power Switch Statistics

Power Switch	Actuations
PMA Actuators	90,893
Camera Pwr Converter	32,278
MCB Power Converter	24,844
Mobility Actuators	15,654
UHF Power	10,257
SSPA A Power	9,021
HGA Actuators	8,945
MTES Power	6,784
IMU Power Converter	6,710
IDD Actuators	6,656
Right Wheel Heaters	4,516
MTES Heater A	3,805
APXS Power	3,016
Left Wheel Heaters	1,476
SDST Power	1,314
MB Power	1,136
HGA Actuators Heaters	556

Power Switch	Actuations
HGA Bearing Heaters	554
RAT Power	550
NavCam Heaters	274
PanCam Bearing Heaters	246
PanCam Warmup Heaters	222
REM Survival Heater A1	68
REM Survival Heater B1	68
REM Survival Heater A2	68
REM Survival Heater B2	68
Front HazCam Heaters	16
MI Heater	8
Rear HazCam Heaters	4
MTES Heater B	3
VME Power Converter	0
SSPA B Power	0
RAT Heater	0
MCB FPGA Heater	0

5.7 Miscellaneous Statistics

IMU Usage	Hours
IMU On Time	N/A, ~3.4x Integration Time
IMU Integration Time	530.190

IMU Power Cycles	3355

Radioactive Sources	Type	Strength at Landing	Strength at EOM	% Remaining at EOM
Mossbauer Spectrometer	Cobalt 57 (gamma ray)	150 mCi	0.00 mCi	0.0
APXS Spectrometer	Curium 244 (alpha particle & x-ray)	30 mCi	17.30 mCi	57.7
Radiothermal Heater Unit	Plutonium 238 (alpha particle)	33.6 Ci / 1 Watt	29.99 Ci/ 0.89 Watts	89.3

6 Rover engineering assessment (prior to dust storm)

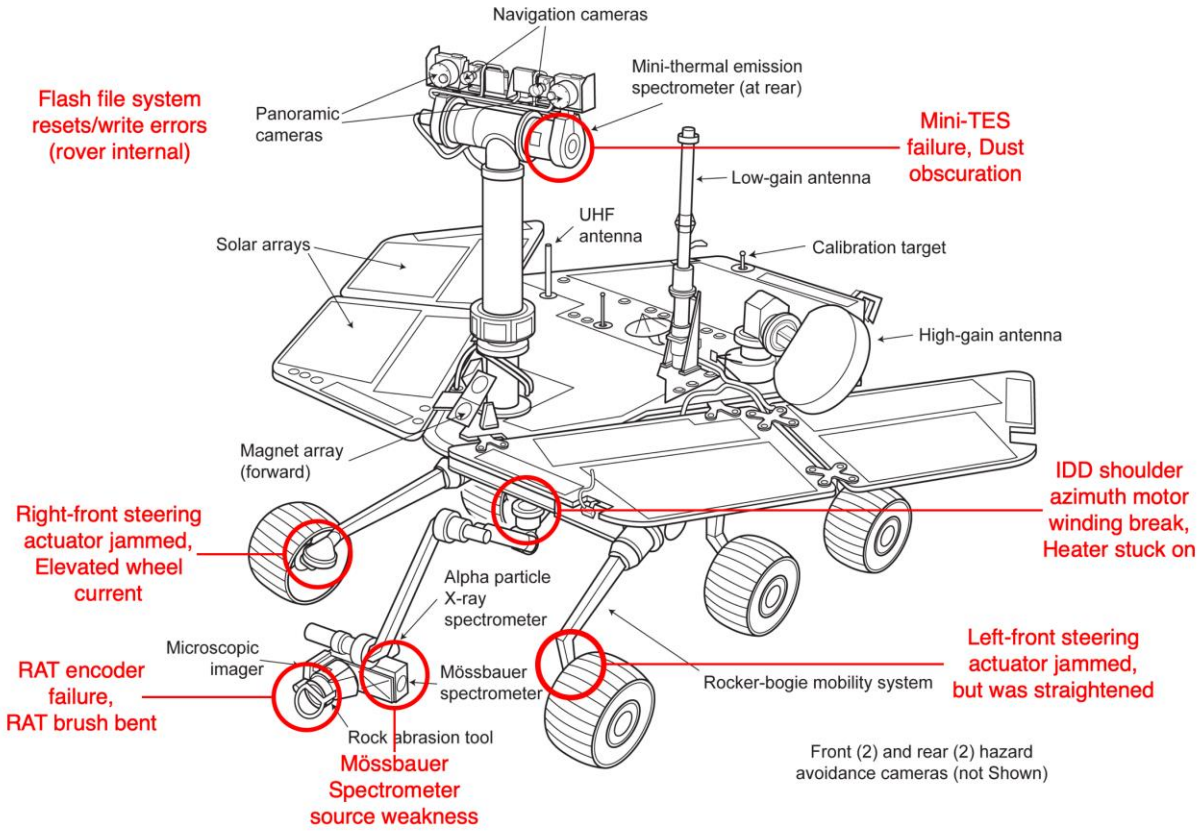

Fig. 6.1. Graphic summary of rover hardware status prior to global dust event and loss of communication.

6.1 Right-Front Steering Actuator

On Sol 433 (2005-04-12), the right-front steering actuator on *Opportunity* jammed. The investigated behavior indicated a gearbox jam and not a motor failure. The wheel was slightly "toed in" within 7° from straight. The rover could effectively steer with the remaining three functioning steering actuators on the other wheels. However, larger arc turns had to be used, and turns-in-place had to be executed more slowly with additional attention when the turn was counterclockwise. A failure of one or more steering actuator with the wheels far from straight would compromise not just steering, but straight driving as well. The project's operational policy was to straighten the wheels at the conclusion of every drive. The rover could always "tank turn" even if all steering was lost as long as the wheels were reasonably straight.

6.2 Left-Front Steering Actuator

On Sol 4750, *Opportunity* experienced a left-front steering stall during a short planned arc. Telemetry indicated that the left-front wheel was steering through most of the approximately 34 degrees it was commanded, but stalled within 0.7 degrees of the final position. Rover flight software declared a stall when the encoders indicated no movement in the steering actuator. The steering current also increased markedly with the stall condition. The wheel is currently toed-out from straight by 33.3 degrees.

On Sol 4763, a repeated set of left-front steering tests on *Opportunity* straighten the left-front steering actuator. This was attempted at 15, 18 21 and 24 volts, but this time with more telemetry sampling. All the commanded steering motions failed except for the very last command that move the wheel to straight ahead. The project drove the rover from this point on without steering the left-front wheel and use only the rear wheels for steering. No clear explanation for this anomaly was identified.

6.3 Right-Front Wheel Drive Actuator

The right-front wheel drive actuator on *Opportunity* had been exhibiting elevated current draw (relative to the other wheels) since around Sol 150 with a significant increase around Sol 1686 (2008-10-20). The explanation for the elevated current was not known. All of *Opportunity's* drive actuators were well past design life by several factors. (See section 5 for the current actuator revolution totals.) This elevated current may have been an indicator of limited actuator life, but this could not be established. Hypotheses as to the explanation included gear train wear, brush wear, starved lubrication, gear train contamination, and indirect effects from the jammed right-front steering actuator, among others.

The project took steps to mitigate the elevated current, including resting the actuator (i.e., not driving when there is no significant adverse effect on science return) to allow lubricants to re-flow, heating the actuator to reduce the lubricant viscosity and driving backward to wear the gear teeth on their opposite face. Driving backward appeared to provide the most effective mitigation. However, driving backward required that the project develop a modified technique for autonomous navigation (AutoNav) as the rover low-gain antenna (LGA) obstructed part of the Navigation camera (Navcam) field-of-view (FOV) when looking backward. The updated AutoNav incorporated a small rover jog at the point of imaging to reveal terrain that otherwise would have had the LGA in the FOV. *Opportunity* had been driving backward predominantly since Sol 1825 (2009-03-12) without issue.

6.4 IDD Joint 1 Actuator

On Sol 654 (2005-11-26), the Instrument Deployment Device (IDD, robotic arm) Joint 1 (Azimuth) actuator on *Opportunity* developed a fault. A winding break in the motor resulted in degraded motor performance. This winding break is believed to be a result of the large temperature excursions that this joint and the IDD Joint 2 (Elevation) actuator experienced as a result of the stuck-on heater (an anomaly discovered upon landing). It was assessed that both Joint 1 and Joint 2 were at elevated risk for another winding break, which could degrade or impede the use of the IDD.

The project positioned Joint 1 with the IDD out in front of the rover and implemented what was called the "fishing stow" position for driving with the end of the IDD (turret head) out in front and above the level of the rover belly pan. This allowed *Opportunity* to continue to drive while allowing effective IDD target placement with the rover providing the required azimuthal positioning lost in Joint 1. This position had been used successfully for many hundreds of driving sols. See section 5 for a summary of IDD actuator usage.

6.5 IDD Flexcable

Encoders for the Rock Abrasion Tool (RAT) had failed. These encoders employed signal lines in the ribbon-like flexible cable (flexcable) that traveled through the five complex joints of the

IDD. It was suspected that years of use of the IDD had resulted in wear and breakage of some of the signal lines in the flexcable.

On Sol 1045 (2007-01-01) the RAT encoder controlling the RAT grind function failed. This encoder signal line, used to detect grind motor motions, was at the outer edge of the RAT flexcable. The project was able to develop a work-around employing motor current to detect RAT grind motor stalls (i.e., lack of motor motion). Extensive investigative testing and resolution development work was performed using the project surface system testbed (SSTB) rover at JPL. RAT grinds could be conducted successfully with this new technique. On Sol 1334, the RAT revolve encoder failed. This encoder signal was the next adjacent set of signal traces in the flexcable. Again, the project was able to develop a work-around employing timed control of the RAT revolve function. On Sol 1759, the signal traces that correspond to *Opportunity's* RAT Z-motion encoder failed, and like the others, an effective work around was developed.

6.6 Rock Abrasion Tool

The grinding head of the Rock Abrasion Tool (RAT) on *Opportunity* was still capable of grinding despite having been used to grind rocks more than 52 times. Approximately 25% of the grind bit remained. The remaining life of the grind heads on the *Opportunity* RAT was difficult to assess, so RAT grinding was treated as a consumable. The ability of the RAT to brush rocks was unaffected by grind bit wear, and brushing capability was effectively unlimited as long as all RAT actuators remain functional. The brush on *Opportunity's* RAT was accidentally bent around Sol 1347 or 1348 (2007-11-07). This degraded performance slightly, leaving a very small "island" of un-removed cuttings in the center of the abraded area. The fractional area covered by un-removed cuttings was less than 10%, and there was no significant degradation to geochemical measurements of the abraded region.

6.7 Alpha Particle X-ray Spectrometer

Both the Alpha Particle X-ray Spectrometer (APXS) and the Mössbauer (MB) instruments contained radioactive sources that decayed in strength over time. However, because the half-life of the ^{244}Cm source used in the APXS is 17.6 years, there was no significant degradation in the performance of this instrument over the lifetime of *Opportunity*. As of mission end, the ^{244}Cm source was at approximately 58% of the strength at landing. The APXS actually provided better data at the end mission than it did on Sol 1 because the background from the MB source decayed away. The APXS was fully functional, with no significant degradation of performance.

6.8 Mössbauer Spectrometer

Declining source strength was an issue for the Mössbauer spectrometer. The half-life of ^{57}Co used in the Mössbauer is 271 days, and the original source strength was about 120 millicuries at landing. Source strength was about 0.001 mCi at Sol 4320. Mössbauer measurements were no longer useful due to the greatly weakened source. The MB was retired from use on Sol 3081 (2012-09-23).

6.9 Mini-TES

In the early (Earth) summer of 2007, a massive dust storm engulfed Mars severely affecting both rovers. Darkened skies threatened the survival of *Opportunity*. One apparent consequence of that storm was that the Mini-TES exhibited significant signal degradation. This degradation was suspected to be the result of dust contamination on the Mini-TES fore-optics (mirrored surfaces) in the Pancam Mast Assembly (PMA). The degradation was nearly 100%. The project

implemented a strategy to open the Mini-TES shroud on most sols, exposing the elevation mirror to the environment with a hope of cleaning from wind events. No cleaning occurred.

On Sol 2550 (2011-03-27), the Mini-TES instrument began to malfunction, providing no telemetry and generating a PMA fault. The Mini-TES was subject to extreme temperatures as a result of the implementation of Deep Sleep to save rover energy. Subsequent extensive diagnostics did not shed any light of the nature of the failure nor were able to get any operational response from the instrument. Rover telemetry did not indicate the Mini-TES was turning on when commanded. The failure appeared permanent. The project declared the Mini-TES instrument non-operational and did not plan any further Mini-TES activities. The Mini-TES survival heaters were subsequently disabled.

6.10 Cameras

All cameras on *Opportunity* continued to operate with excellent performance. On Sol 1084, a bad pixel appeared in the left front hazard avoidance camera (Hazcam) but subsequently went away (recovered). If the bad pixel had persisted, internal camera functionality for bad pixels could be activated in the camera to correct for the defect. Minor dust contamination existed on all camera optics, but the effects were removed by calibration. The Pancam and Microscopic Imager (MI) were fully functional, with no significant degradation of performance. The effects of minor dust on the optics could also be corrected by normal calibration procedures.

The project was concerned about actuator lifetime and in particular for the PMA camera elevation bar. This high-use actuator is critical for camera operations. To mitigate the risks from the loss of use for this actuator, the project modified the camera bar stow position from −90° to −17°. This position still provided protection against air-fall dust but maintained a functional (science and mobility) field of view for both the Pancam and Navcam camera systems in the event of actuator failure while stowed.

6.11 IVP Vector Error

The Inertial Vector Propagator (IVP) quaterion used to estimate Earth's position relative to the Sun was based on the Earth geocenter instead of the Earth-Moon barycenter. This caused a high-gain antenna (HGA) pointing error that had a sharp peak near Earth-Mars opposition (closest approach). The error magnitude increased on each successive opposition (every ~2 years). It was of significant, but manageable concern during opposition in 2014. Opposition in 2016 was also manageable. However, Opposition in 2018 and later was predicted to have pointing errors large enough to preclude rover HGA communication for periods of two or more months. Although the use of the low-gain antenna (LGA), or instituting a period of forward commanding through the relay orbiters would allow operation through these periods, the project was in the process of a new flight software build to correct these errors. That new flight software was developed but never uploaded to the spacecraft.

6.12 Flash File System

Opportunity experienced a series of "amnesia" events where the rover's non-volatile flash file system would not mount and volatile RAM memory would be used instead. It was referred to as amnesia because the rover would not retain any telemetry after it shut down to sleep each sol. Amnesia events first occurred on Sol 3082 (2012-09-24). Another Flash anomaly behavior involving write errors had also been observed. Flash-related memory write errors began to occur on Sol 3235. These events resulted in a reset of the rover. None of these events were a health or

safety risk for the rover. They did potentially result in some lost science data. The project continued to investigate this, but no cause was ever identified.

During the 9th extended mission, Flash memory continued to degrade. The project created a new flight software build to mask off part of Flash memory and reformat the remaining portion. That was insufficient to enable continued use of Flash. As a result, the project disabled the use of Flash and instead began to rely on the use of random-access memory (RAM) for volatile data storage. This required that the rover stay awake until each communication pass to return data to Earth as all stored data were lost when the rover slept. This required some important operational changes. Science activities were typically moved later each day just ahead of a communication pass. Late or overnight activities were limited to the APXS alone (the APXS has internal non-volatile storage). Large data activities such as a large panorama had to be split up and collected over multiple sols at similar times of day. The project continued to operate the rover in this persistent RAM mode through end of mission.

6.13 Other Issues

Occasional warning messages indicated that some commands transmitted to the Microscopic Imager on *Opportunity* were corrupted. In all but one instance, an automatic re-commanding had been successful, resulting in no loss of data. The symptoms may indicate temperature dependence in that interface, or partial cable delamination. The occurrence was infrequent and showed no sign of becoming more common, but the project continued to track it.

Actuator motor lifetime was a concern, because the brush motors used in virtually all rover applications wear out over time. Each motor was qualified to operate for at least 10 million cycles. The Pancam Mast Assembly (PMA) azimuth actuator was a particularly high-use application, however, it exceeded this limit during the extended mission and continued to operate normally. Section 5 summarizes the actuator usage for both rovers.

6.14 Other Components

The non-volatile EEPROM memory on the rover had an estimated life of between 30,000 to 300,000 write cycles per sector. The majority of EEPROM sectors had not been used on *Opportunity*. There was only one EEPROM area with a write fault. An unused rover sequence overlayed that area to prevent further use.

The waveguide transfer switch in the X-band telecom system was rated at a lifetime of 20,000 cycles. Approximately 8430 cycles had been performed. The CXS-1 switch did exhibit some anomalous behavior. The project made a fault protection parameter change to never actuate this switch with minimal impact to rover fault response. All remaining elements of the both the X-band and UHF telecommunications systems were functioning fully.

Opportunity's Li-ion batteries continued to show a slower rate of degradation than identical units in ground tests. The last estimate of capacity for the rover's batteries was approximately 17.8 amp-hours (Sol 4320). This corresponded to approximately 83% of the original battery capacity. Predictions estimated useful battery life would extend beyond Sol 15000.

7 End of mission assessment[1]

7.1 2018 Mars Planet-Encircling Dust Event at Perseverance Valley

A planet-encircling dust event (PEDE) began near *Opportunity* in June 2018. Several factors contribute to dust storms on Mars. The orbit of Mars is much more elliptical than that of Earth, with perihelion at 1.38 Astronomical Units (AU) and aphelion at 1.67 AU. The planetary tilts are similar, with Mars' tilt of 25.2 degrees - less than 2 degrees different from Earth's 23.4 degrees - so Mars undergoes seasonal changes like Earth; however, seasons are more extreme in Mars' southern hemisphere, where summer coincides with perihelion while winter coincides with aphelion. There are also differences in albedo on the Martian surface – some areas on the surface are light while other areas are dark. The darker areas heat more, especially near perihelion, and the polar ice caps sublimates every Mars year, seasonally increasing the surface pressure (Zurek, R., 1982). All of this amounts to increased wind on Mars during southern spring and into summer, and the possibility of dust storms during those seasons. Sometimes, roughly every 3 Mars years and for reasons not entirely understood, the dust storms can grow in such strength and size that they encircle the entire planet (Shirley, J., 2015). Dust particles are typically 2-4 micrometers in diameter (Lemmon et al., 2015).

Martian winds cause the surface dust to be lofted into the atmosphere, increasing the atmospheric opacity (Tau) initially and then increasing the dust accumulation on the solar panels (array dust factor) during saltation (Lemmon et al., 2015; Stella and Hermon, 2010). Dust factor is a measure of how much dust blocks solar energy from reaching the Solar Array cells; i.e., how much dust is on the Solar Arrays. Dust factor takes on a theoretical value between 1.0 (perfectly clean arrays) and 0 (completely dirty panels). During the decay phase of dust storms, dust factor is the greatest concern for power generation.

1. Dust storm operations for solar-powered spacecraft requires a careful balancing act between four distinct elements:
2. Power Management - Maintaining onboard power levels to prevent tripping low-power system fault response and damage to the batteries
3. Thermal Management - Maintaining the internal temperatures for electronic health
4. Ground Communications - Ensuring the ground maintains the most current knowledge of the dust environment
5. Science – Dust Storms are scientifically rich events that provide insight into the dynamics of the Martian atmosphere. They are also beneficial for engineering for the design of new robotic missions and/or human-rated systems for future crewed-missions

Depending on the type and strength of storm, solar-array energy production can fall dramatically between communication sessions, depending on the peak Tau and magnitude of accumulated dust (dust-factor) on the solar panels.

[1] Text in this section is modified from *Staab, M. S., Herman, J.A., Reich, K., Sridhar, V., and Nelson, R.W. (*2019) "MER *Opportunity* Dust-Storm Recovery Operations and Implications for Future Mars Surface missions," *IEEE Aerospace Conference,* Big Sky, MT, March 7-14, 2020.

An abbreviated timeline of the environmental conditions over Perseverance Valley and reported S/C state from the Sol prior to the first indication of the storm through last contact is shown in table 7.1. Data for Sols 5108 and 5110 are missing because the communications for these Sols were removed from the vehicle in an effort to conserve dwindling available onboard power and with no non-volatile memory, information cannot be saved between rover shutdowns. Over the course of eight Sols, the produced Solar-Array Energy dropped 96.7% from Sol 5103 with a 73.2% drop in battery State-of-Charge (SOC) and 1668% increase in observed Tau. Within this period, *Opportunity* achieved a number of mission records for power, including lowest recorded battery SOC, Solar Array Energy production, Solar Array Current (0.25A, with 0.2A required to wake-up from "Deep Sleep"), and Bus Voltage (26.6V, with 24.0V the threshold for tripping Low-Power Fault response).

Table 7.1. 2018 PEDE Dust-Storm Progression

Sol	Tau	Energy (W-hr.)	SOC (A-hr.)
5103	0.611	660	11.2
5104	1.548	463	12.1
5105	1.020	462	8.9
5106	2.115	365	7.9
5107	4.9	123	10.4
5109	8.7	28	6.7
5111	10.8	22	3.0

Due to the shear intensity and rapid growth of the 2018 PEDE storm, the MER operations teams was unable to move *Opportunity* to a more ideal tilt to ride out the dust storm and, instead, proceeded immediately to removing as many non-essential activities onboard as possible. Beginning with planning for Sol 5107, the following actions were taken:

1. All *Odyssey* overflight were removed from the S/C (favored *MRO* because overflights were earlier in the Sol and better for power – 13:30 LST vs. 18:30 LST)
2. All MRO flights were shortened to six minutes(minimum pass duration) and link-rate dropped from 128Kb to 32Kb (higher link margin to ensure strong link with orbiter – priority was receiving crucial data for planning, not the volume of data obtained)
3. All non-commanding X-band windows (when team didn't send data to the S/C) shortened to five minute Low-Gain Antenna (LGA) windows (minimum window time and powers down vehicle early to conserve batteries; additionally, doesn't draw extra power to move High-Gain Antenna (HGA) gimbals)
4. Commanding X-band windows shortened to 10 minutes (balance between ensuring sufficient margin to get sequences onboard and power down early to conserve power)
5. Only Tau images and BCB histories allowed, taken on Sols when MRO overflights are planned (due to *Opportunity* operating only out of the RAM-only File System, whatever data was captured must be downlinked before shutting down)

As the likelihood of losing contact with *Opportunity* became more apparent, MER's flight team made the decision to swap from our traditional uplink-loss timer of 10950 minutes to 40000 minutes. An uplink-loss timer is simply a counter onboard the S/C that counts down monotonically and, upon expiration, asserts a System Fault Response (SFP) called Uploss. A discussion of this SFP response will be discussed in the following section, but essentially the timer is a watchdog to prevent against unexpected loss of communication with the ground or

failure of a communication string on the rover. The choice to transition to the larger timer was the result of expecting to lose contact with the vehicle and reduce the chance of requiring a recovery from Uplink loss, a much more challenging S/C recovery compared to Low-Power Fault.

Opportunity made final contact on June 10, 2018 at 17:05 UTC. Following unsuccessful attempts to hear from the vehicle the following two days, nominal operations were suspended, and the team transitioned to recovery operations.

7.2 Recovery Efforts

Prior to any recovery strategy development, the team required a complete understanding of the predicted power and thermal environments, along with expected telecom performance and MER fault and mode behaviors, to understand both the duration of the possible recovery window and how developed recovery strategies would adapt to the changing environment. With these predictions, three strategies were developed encompassing the steps to re-establish contact with the vehicle: (1) determine the vehicle's onboard state (power, thermal, fault protection), (2) transition the vehicle to known, commandable state, and, (3) return the vehicle to nominal science operations. These strategies were developed concurrently with ground-based testing, which both ensured integrity of the developed strategies and informed the strategy's development.

7.2.1 Power Environment Estimation

MER's power team conducted analysis of the predicted power environment for *Opportunity* immediately following loss of contact through the decay phase of the storm. Analysis was broken into three sections: solar insolation trending through the end of summer, Solar Array energy prediction for a range of dust factors through the end of summer, and a review historical dust factor data to identify L_s periods cleaning may occur. As the timing of the 2018 storm was very early in the southern spring (L_s 191) and atmospheric opacity was greatly elevated (Tau >> 3.0), the flight team expected the atmospheric opacity to exceed safe operating levels (Tau > 2.0) for at least two months. The advantage, however, of a storm shortly after spring equinox was solar insolation levels would remain favorable, from a power perspective, for recovery over an extended period of time (~9 months) and environmental temperatures would be more favorable.

Analysis of MER's fault modes indicated the minimum energy required for contact was > 249 W-hr/Sol and > 300 W-hr/Sol for stable recovery. At the end of the two month decay period to Tau > 2.0, the goal was that the solar arrays would become clean enough to generate at least 300 W-hr./Sol, the amount of energy/sol required to sustain fault recovery operations. Unfortunately, "clean enough" meant a dust factor of 0.6 (*i.e.*, 60% of the sunlight reaching the solar arrays is able to penetrate the dust layer), which was approximately how clean the solar array were when contact was lost. After a two-month decay in atmospheric opacity, it was believed the dust factor would likely be much worse than 0.6, as the dust lofted into Mars' atmosphere fell back to the surface. As shown in Figure 7.1, a dust factor greater than 0.6 guaranteed the minimum energy required for stable recovery. A dust factor of 0.4 would not provide the minimum energy for consistent contacts. Therefore, it was speculated that *Opportunity* required some amount of cleaning before the end of southern summer to make contact with the ground.

Finally, a review of the historical array dust factor trends (Herman *et al.*, in preparation) – over 7 Mars years' worth of observations – indicated that there was a high probability of array dust cleaning events from Ls 290 (11/17/18) to Ls 320 (1/7/19). It was possible *Opportunity* had enough energy to safely "hibernate", but not sufficient to communicate without eolian removal of dust from the solar arrays.

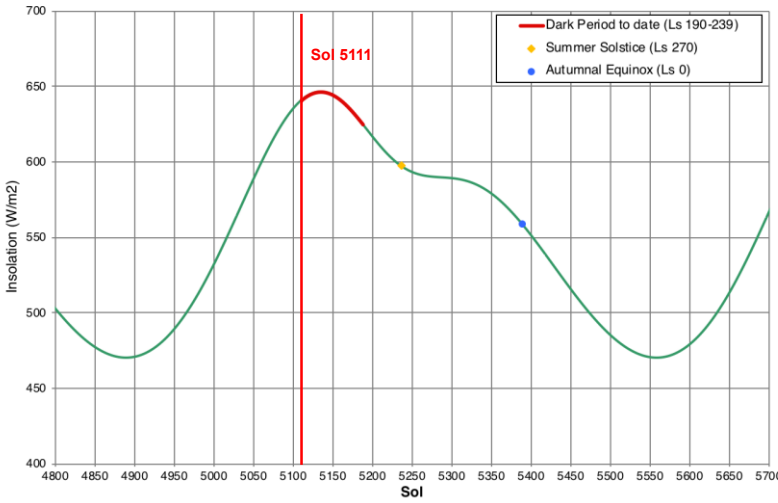

Fig. 7.1 *Opportunity* power estimates through autumn equinox (df = 0.6)

7.2.2 Thermal Environmental Estimation

The Mars Exploration Rover's Warm Electronic Box (WEB) was designed with low thermal conductivity composites and highly efficient opacified aerogel insulation. The internals and externals surfaces of the WEB walls were designed to minimize the radiative heat loss to the environment. Within the rover, eight RHU (Radioisotope Heater Units, 1W each, 6 on the batteries and 2 in the WEB) produced heat to keep the electronics warm. Additionally, there were survival heaters with mechanically activated thermostats designed to prevent the electronic hardware from dropping below minimum allowable flight temperatures (the temperature range the hardware must be kept within to prevent damage). Internally, MER had three (3) circuits for the heaters: the Rover Electronics Module (REM), the batteries, and the Mini-TES. Additionally, two wax-actuated thermal switches prevented the rover batteries from overheating. Externally, the rover had heaters on external actuators and cameras (commanded heaters used during operations). Furthermore, the external heaters possessed thermostats that prevented the hardware from overheating.

For the 2018 PEDE Storm, the goal of the thermal analysis was to characterize the possibility of triggering REM Survival Heater and Battery Heaters during recovery efforts. Using Systems Improved Numerical Differencing Analyzer (SINDA)/FLUENT, thermal analysis was performed to predict the estimated rover internal temperatures, determining the point, thermally, when the rover temperatures would drop below allowable flight temperatures. The model incorporated the albedo, thermal inertia, *Opportunity's* topographical elevation, and latitude. The analysis assumed the rover batteries were offline beyond Sol 5112, modeling the "worst case probable" scenario for conservatism. Furthermore, to mimic the dust storm and its effect on the environment, the model assumed low atmospheric opacity for colder temperatures (again, for conservatism). With the battery offline assumption, the sole heat source inside the WEB was from the RHUs, each producing ~1W of thermal power.

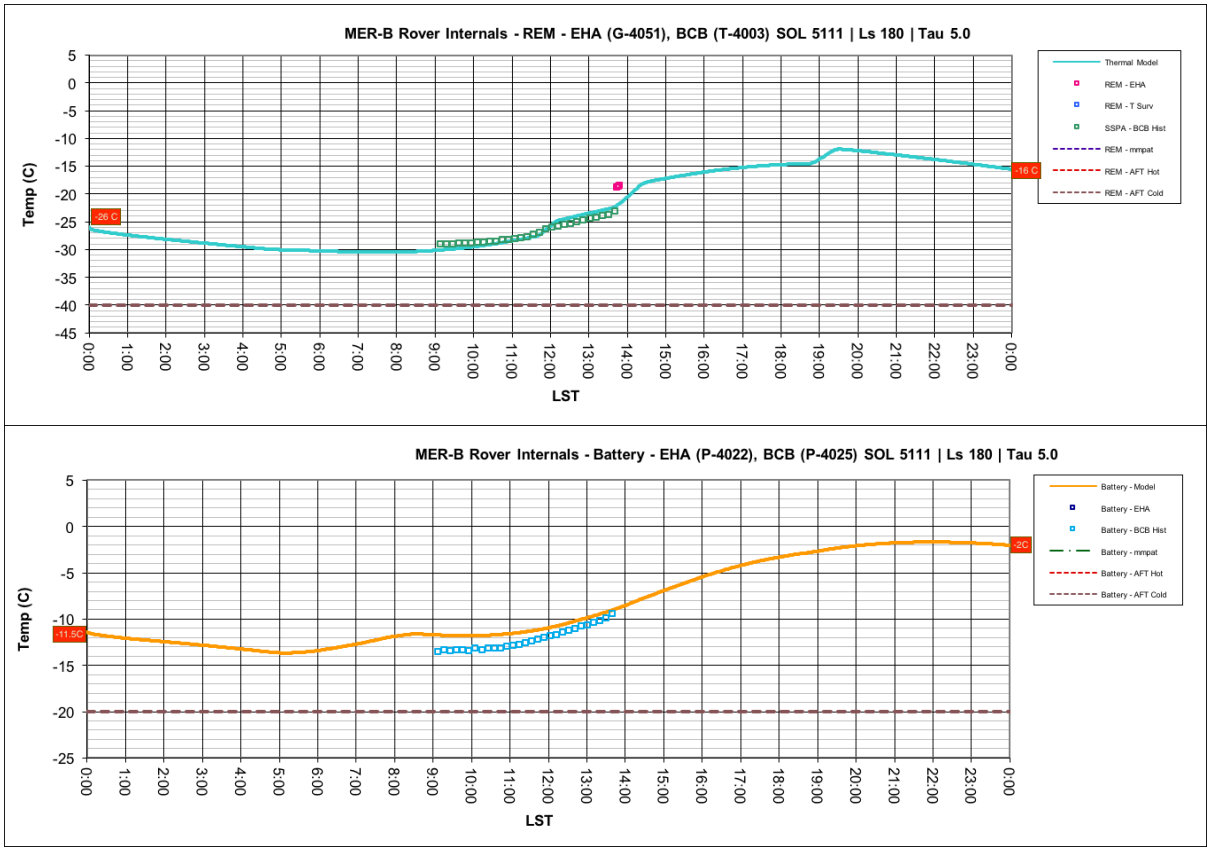

Fig. 7.2 Quasi-steady state thermal analysis of *Opportunity* REM and batteries

Figure 7.2 summarizes the thermal data of the Rover Electronics Module and batteries from the last downlink against the SINDA Thermal model run. Though the actual Tau was recorded to be over 10, the model ran with a Tau of 5.0 as it correlated well with the received data (this is due to error and uncertainty in the SINDA model). Recall, the results of these thermal simulations assumed no thermal energy additions to *Opportunity* except from the RHUs. For added conservatism, the simulations were run again with the Tau forced to 0.5, which had the effect of raising the maximum Sol temperature and lowering the minimum overnight temperature. From this simulation, even under a worst case scenario, REM temperatures settled to a quasi-steady state of -27 C, with battery temperatures settling to -9.3 C. This indicated that the PEDE storm created a thermal blanket that diurnally kept the REM in a -27 C to -36 C swing with batteries temperatures bounded between to -6.5 C to -18 C.

The goal of the thermal study was to predict when the REM and Battery survival heaters would engage as the PEDE storm dissipated. MER's Solar Arrays possess a high (IR) emissivity and, with "clear skies", the rover becomes very cold at night. Initial thermal analysis (using Environmental Data Files for Ls270 and Ls0) showed no heater turn-on at Ls270 (Sol 5236, 10/16/2018); however, the model indicated that the heater would engage by Ls0 (Sol 5390, 3/23/2019). To obtain a more definite initial heater turn-on date, analysis between Ls270 and L0 was required. In nominally operations, thermal models only used Environment Files for Ls0, Ls90, Ls180 and Ls270. To obtain the increased fidelity, additional Environment Files were

created, built in 10-degree deltas of Ls from Ls270 to Ls0. With the new environment files (Ls280, Ls290, Ls300, Ls310, Ls320, Ls330, Ls340, Ls350), SINDA Thermal models were run at each Ls with Tau values of 0.5 and 1.0. From these simulations, it was predicted that for a Tau of 0.5, the battery heaters would engage between Sol 5334 (1/25/2019) and Sol 5352 (2/12/2019) and the REM heaters between Sol 5352 (2/12/2019) and Sol 5371 (3/4/2019). For a Tau of 1.0, the battery heaters would engage between Sol 5371 (3/4/2019) and Sol 5390 (3/23/2019) and the REM Heaters between Sol 5371 (3/4/2019) and Sol 5390 (3/23/2019).

Given the severity of the PEDE storm, the engagement of any of the heaters, particularly the REM survival heaters, would have placed the vehicle into an unrecoverable death spiral. As the survival heaters engaged to warm the cold internal environment, the increased load, due to an already challenging power environment, would almost certainly trip an undervoltage of the bus, shedding the loads on the spacecraft – the exact opposite effect of the survival heaters. This scenario would play out over and over again as the rover approached winter until steadily dropping overnight temperatures finally caused permanent hardware damage to the sensitive avionics' equipment. As such, the team identified, from this thermal analysis, *Opportunity*, at best, had until March to be back under sequence control to survive.

7.2.3 Telecom Analysis

Analysis of expected telecommunications performance was conducted to determine expected signal strength from *Opportunity's* LGA for commanded "beeps" and autonomously executing fault windows with the Deep Space Network's (DSN) array of 34 and 70 meter antennas. The team required two pieces of information:

1. Expected Carrier-Power-to-Noise (Pc/No) from "beep" and fault window carrier signals, minimum thresholds for detection, and observability window of those signals
2. Frequency range from autonomous contacts, based on ATLO data and modeled Auxiliary Oscillator baseplate temperatures

Knowledge of the Pc/No values informs the expected values for signal detection in the VSR plots used during MER's listening campaign. During the early days of the recovery effort, commanded "beeps" from the vehicle were expected to 30 dB-Hz with a 34-meter DSN station and 36 dB-Hz with a 70-meter DSN station (70-meter dishes provide 4x the collection area of a 34-meter station, equivalent to 6 dB in additional gain). For autonomous executing fault windows, the expected Pc/No values were 27 dB-Hz and 33 dB-Hz for 34-meter and 70-meter dishes, respectively.

Note: Autonomously executing fault windows are suppressed by 3 dB due to modulation of data on the carrier signal's subcarrier.

Additional analysis showed the minimum Pc/No threshold for any signal was approximately 18 dB-Hz. From this threshold constraint, the telecommunications team determined autonomously execution fault windows would be unresolvable past Sol 5362 (February 23, 2019) and beeps past Sol 5461 (May 5, 2019) with 34-meter dishes. On the 70-meter dishes, autonomously executing fault windows would be unresolvable on Sol 5490 (July 5, 2019) with "beeps" well beyond that point (due to upper limits of analysis).

Previously performed thermal analysis was used to determine the expected frequency range the spacecraft would transmit at for autonomously executing fault windows, based on the temperature of the Auxiliary Oscillator baseplate. Using conservative estimates for baseplate

temperature (0°C to -40°C) and results from Auxiliary Oscillator performance in ATLO, expected transmission frequencies centered at 8.4353 GHz +/- 100 kHz. These values were communicated to JPL's Radio Science team and used for post-processing of VSR recordings employed during MER's Listening Strategy (discussed in a subsequent section).

7.3 MER fault behavior and modes

The operations team identified three possible spacecraft states during the dust storm that would be recoverable: Low Power Fault, Uplink Loss Fault (Uploss Fault), and Mission Clock Power Loss Fault (MCLK Fault). MCLK Fault is the highest priority system fault response in terms of onboard arbitration, followed by Uploss Fault and then Low Power Fault. Arbitration allows the highest priority active system fault response to take action, while the other conflicting responses are disallowed to take action until the ground stops the higher priority response. Only Uploss and MCLK Faults were determined to be possible after 28 days of no contact with *Opportunity*, since Uploss would take action at that time and preclude the Low Power Fault actions. The recovery commanding strategy was designed to cover each of these possible fault scenarios simultaneously, in order to expedite the reestablishment of communication and return to operation before the arrival of Martian winter. Each of these system faults places the spacecraft into a communications mode that autonomously spawns Direct-To-Earth (DTE) communication windows over X-Band RF. The windows were each configured to use the Small Deep Space Transponder (SDST) X-Band radio, either the primary or backup Solid State Power Amplifier (SSPA), and the Low Gain Antenna (LGA). Commanding and telemetry data rates were configured to be as low as possible for the most reliable data transfer: 7.8125 bps for uplink and 10 bps for downlink. The main difference in DSN configuration needed for listening for the windows was polarization: Right (RCP) or Left (LCP) Circular Polarization, depending on the active fault's comm scheduling.

7.3.1 Low power fault

In the event of interruption to system power, the fault protection system is designed to shed loads and place system into a low power mode capable of restoring communication in a timely manner with minimal power consumption. All sequenced activities are terminated upon entry into the mode, and the communication behavior is configured to wake up the rover for a comm window at 11:30 GST (Generic Solar Time, or time since last midnight in Mars hours) each sol. All comm windows scheduled use RCP polarization, narrowing the search-space for a low power spacecraft recovery. Note that nominal comm windows previously loaded in nominal operations are not allowed to execute in this mode. The following three fault monitors trigger entry into a Low Power Fault:

1. Battery Offline Imminent: If any battery cell drops below 2.9 volts, the Battery Control Board (BCB) informs FSW that battery discharge will be disabled in 60 seconds. Unlike with the other fault triggers, the FSW takes immediate action to shut down the system in an expedited fashion prior to the battery being taken offline.
2. Battery Offline at Boot: If either or both batteries are offline during FSW initialization, FSW will declare a low power fault and remain awake until autonomous shutdown behavior takes effect. Note that the rover may be running off solar power and/or a single battery in this scenario.

3. Rover Power Distribution Unit (RPDU) Power-On Reset (POR) Detected: If FSW detects that power has been interrupted to the RPDU, FSW will declare a low power fault and remain awake until autonomous shutdown behavior takes effect. However, this fault trigger was disabled for *Opportunity* as part of the Deep Sleep behavior implementation, since Deep Sleep intentionally disconnects the batteries each evening before shutting down for the night, and the rover detects that the RPDU power has been interrupted during FSW initialization the following morning.

7.3.2 Uplink loss fault (uploss fault)

Uploss is designed to place the system into a safe communication configuration in the event that uplink has not been received from Earth by a certain absolute time. In normal operations, ground includes a command to advance the uploss time for action with each activity plan uplinked to the spacecraft, so that the time for action always stays in the future. In the event that uplink cannot be established by the time for action, sequence control is terminated and the spacecraft transitions to a communications mode that autonomously schedules X-Band DTE windows at 11:30 GST each sol, alternating between RCP polarization on the primary SSPA and LCP on the backup SSPA configurations each sol. In this communications mode, nominal X-Band comm windows previously uploaded are not allowed to execute, but UHF orbiter relay comm windows are permitted.

As previously mentioned, the uploss time for action was advanced to 40,000 minutes (27 days, 18 hours, 40 minutes) from the last successful uplink to the spacecraft, in order to prevent the uploss fault from occurring. However, given that the ground team was unable to establish communication within 28 days of the last commanding, we can assume that the uploss fault would have been detected if the FSW were to wake up. Given that system arbitration prioritizes uploss fault actions over low power, we ruled out the possibility of the system being in a low power fault state during recovery attempts after passing the uploss time for action.

7.3.3 Mission clock power loss fault (MCLK fault)

The MCLK Fault response is designed to reestablish communication with Earth in the event that power has been interrupted to *Opportunity's* mission clock (MCLK) and time has been lost. As the battery depletes past the threshold for disabling battery discharge, the last system to go offline is the MCLK FPGA, which maintains spacecraft time (seconds since J2000 epoch) and alarm clock wakeup functionality. If the battery voltage drops below 16 volts, the mission clock register cannot continue incrementing.

Upon restoration of power, the mission clock register initializes to 0 seconds and resumes counting up, and the alarm clock register initializes to 600 seconds and starts counting down. 10 minutes later, the alarm clock register hits 0 seconds and triggers avionics to power on. If the batteries are sufficiently charged to allow for discharge, or if the solar panels are collecting enough power to support avionics, the flight computer starts up and initializes FSW. However, given that the dust storm took months to abate, a scenario where power can support booting avionics within 10 minutes of the MCLK power being restored was unlikely. Each time the alarm countdown reaches zero, the alarm resets to a "snooze" value of 97,200 seconds, or 27 hours. This cycle of alarm clock expiration would repeat until power can support avionics operation. During FSW initialization, FSW checks the status of the MCLK FPGA to determine if power has been interrupted to the MCLK. If FSW determines that MCLK power was lost at

some point in the past, the MCLK is set to a "recovery time" value. The last known recovery time value saved in flight was 596287876 seconds, which corresponds to 2018-327T23:34:51.636 SCET, or 09:44:16 GST. After reseeding the MCLK, FSW initialization continues and the MCLK Fault response runs.

The MCLK fault response places the rover into a shutdown/wakeup cycle that searches for a time period when the sun is up and solar power can support DTE communication with Earth. During the first wakeup, the rover checks if at least 1.2 Amps are being generated by the solar panels. If so, the rover schedules a DTE for one hour in the future, and the rover stays awake until the time of the window, as long as at least 1.2 Amps of current are maintained on the solar panels. Otherwise, a wakeup is scheduled for four hours in the future, and the rover continues waking up every 4 hours to check if the solar panels are generating sufficient power. Each time a comm window executes, the configuration alternates between primary SSPA on RCP and backup SSPA on LCP. Note that nominal windows previously loaded by ground are not allowed to execute in this mode.

7.4 Recovery strategies

The MER team developed a strategy to establish the steps, resource needs, and commanding options to recover *Opportunity* from the dust-storm and return the vehicle to nominal science operations. The overall strategy covered four topics:

1. Listening Strategy: Steps and processes from loss of communication through initial contact, fault mode determination, and fault window characterization
2. Recovery Strategy: Steps and processes to return the rover to nominal SCM and CBM modes
3. Re-commissioning Strategy: Steps and processes to characterize the health of the rover and its systems prior to returning to unconstrained science operations
4. Ground-analyses and Testing: Steps and processes related to characterization of fault behaviors and testing of recovery products from CETB and SSTB

7.4.1 Listening strategy

The MER Listening Strategy consisted of the steps and processes from loss of communication through initial contact, fault mode determination, and fault window characterization. Depending on the current state of the vehicle (power, thermal, and S/C mode), contacts from *Opportunity* may range from consistent and easy to predict to sporadic and difficult to predict. The Listening Strategy was designed to ease identification of a contact from the vehicle and aid in identification of the running S/C fault mode that implied the characterization of future contacts from the vehicle.

The Listening strategy consisted of two unique and interconnected techniques: passive and active listening. The first technique employed the array of ground-based receivers with the Deep-Space Network (DSN) to passively "listen" to all signals emanating from Mars. Very-Long Baseline Interferometry (VLBI) Science Receivers (VSRs) were utilized as the recorders, provided by the Radio Science ground at JPL. VSRs are wideband, open-loop receivers with the necessary frequency range required to locate *Opportunity's* unknown and moving carrier frequency. As previously noted, the transmitted frequency depends heavily on the temperature of the Auxiliary Oscillator crystal in *Opportunity's* telecommunication system (hence the wideband requirement) and may move significantly during a transmission window as the temperature of

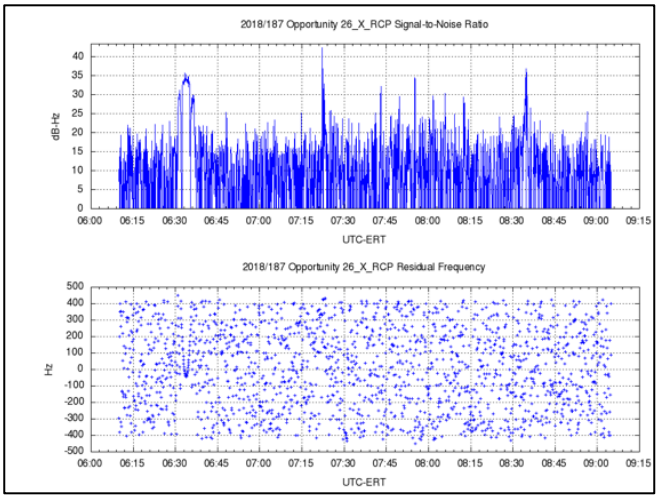

Fig. 7.3 *Opportunity* post-processed VSR recording

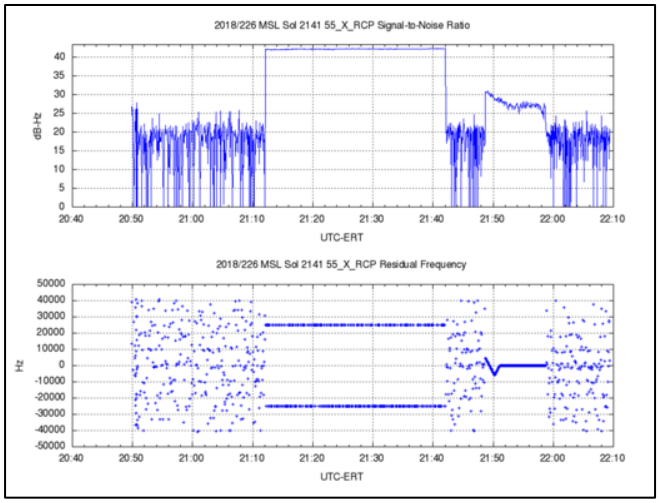

Fig. 7.4 MSL VSR Beep Test

the oscillator warms up (hence the open-loop requirement). VSR recordings were made by the Radio Science team on a best effort basis from 08:30 – 13:30 Local Solar Time (LST) for *Opportunity*, so long as the recordings did not interfere with the currently tracked asset(s) by the station. The recording period corresponded to the most likely time of Sol when *Opportunity* would have sufficient solar energy to execute a MCLK fault (recall, MCLK windows execute based on environmental conditions, so there is a temporal factor as to when the windows execute). Following each recording, the Radio Science team post-processed the file against the last-known *Opportunity* rest frequency (Best-Lock Frequency or BLF) for dissemination to the MER team for further analysis.

In parallel, an active technique commanded a single "beep" every Sol from the rover during the known LPF and Uploss fault window at 11:30 Generic Solar Time (GST). GST is a rover-specific time reference maintained in Flight Software (FSW) to indicate the current local time. The GST reference was used greatly in the implementation of "Deep Sleep," a change to *Opportunity's* FSW to force the S/C to disconnect its batteries from the bus every night due to a stuck-on IDD shoulder joint heater. Beeps correspond to frequency-modulated carrier tones, used first as indications of critical events during EDL and, during surface operations, by the flight team to indicate successful handover from one Sol's "master" sequence to another. Beeps consumed a minimal amount of power, and as the beep sequence was already onboard *Opportunity* prior to loss of contact, this active commanding technique provided a second avenue for making contact with the S/C during the early days of the recovery effort. As an added bonus, the execution of a beep would shut the vehicle down earlier than the executing fault window, preserving precious onboard power.

An example of a processed *Opportunity* VSR file provided by JPL's Radio Science team is shown in Figure 7.3. While chaotic at first glance, a great deal of information may be gleaned from the image when knowing what patterns to look for. For example, both the carrier and sub-

carrier lobes from the Mars Reconnaissance Orbiter (MRO) are present in the Power-Spectral Density (PSD) plot, along with the Doppler-shifted track of the spacecraft's orbit in the frequency plot. Patterns like these are highly indicative of orbiting spacecraft and can easily be disregarded as not emanating from a surface mission.

To properly calibrate the flight team to the expected patterns from *Opportunity*, a VSR test was conducted with the Mars Science Laboratory *Curiosity.* As Figure 7.4 illustrates, the first prominent signal in the plot corresponds to a Direct-to-Earth (DTE) transmission from *Curiosity's* High-Gain Antenna (HGA), similar to a fault window transmission from *Opportunity*. An equally important indication from the DTE transmission is the presence of a 25kHz modulated subcarrier, which is identical to the expected subcarrier from an *Opportunity* fault window. The second signal in the VSR plot corresponds to a beep; notice the change in both the PSD (beeps are transmitted from the Low-Gain Antenna (LGA) rather than HGA) and Doppler-residual plots. As beeps are two-way coherent signals – beeps are transmitted from a DSN-generated reference frequency provided by the project – the expected Doppler-residual should be approximately zero. This test demonstrated two important pieces of information: 1) commanded beeps from *Opportunity* should have a near-zero Doppler-residual and 2) autonomous contacts from *Opportunity* should indicate a 25kHz subcarrier AND 3 dB-Hz suppressed signal in the PSD plot.

From analysis of *Opportunity* modes and possible fault responses, which are beyond the scope of this paper, the MER team developed the following set of criteria for confirming a positive contact from *Opportunity*:

1. **Observed Carrier Power:** Carrier-Power-to-Noise (Pc/No) for a beep is expected around 30 dB-Hz for a 34m DSN station and 35 dB-Hz for a 70m DSN station (based on telecommunications analysis previously performed). Vice versa, a DTE signal from an autonomous fault window will be 3 dB-Hz suppressed from the expected carrier values (27 dB-Hz for 34m station and 32 dB-Hz for 70m station).
2. **Observed Doppler Residual:** Commanded "beep" exhibits little to no Doppler residual as beeps are two-way and sweep completed prior to radiation of command. Vice versa, a DTE exhibits +/- 25kHz Doppler residual due to 25 kHz subcarrier at *Opportunity* fault rate of 10 bps. Doppler residuals may not be exactly centered at BLF due to uncertainty in Auxiliary Oscillator temperature and oscillator warming during DTE transmission
3. **Time of Signal Receipt:** For LPF or Uploss fault DTEs contacts, start of signal corresponds to ~11:30 GST. For MCLK contacts, start of signal may not necessarily correspond to 11:30 GST as the window is highly dependent on environmental conditions and the delta between true LST and what S/C "thinks" is true LST. Commanded beeps should occur very near the expected beep time
4. **Signal Duration:** For commanded beeps, expect 5 minutes; for LPF & MCLK, expect 40 minutes (if power to support); for Uploss, expect 30 minutes (if power to support)

Following confirmation of first contact, the team would proceed based on the type of contact. If a beep was detected first, the team could continue to attempt to send beeps for several days at approximately 11:30 GST, forcing the vehicle to continue to power down early to save power. This was a consideration during the worst part of the dust storm if *Opportunity* made contact, allowing the team to monitor contacts from the vehicle while preserving power until the observed Tau from orbit dropped sufficiently to begin the process of recovery. If a DTE was

detected first, the team would proceed to determine the actively running fault mode using the flowchart developed in Figure 11. The flow chart took all possible fault modes into consideration, swapping of window polarization, and partially observable window durations (i.e., DTE windows < 30 minutes in duration). At minimum, two consecutive contacts were required to correctly identify the running fault mode. Should a window be missed, the process started from the beginning, requiring two consecutive contacts before proceeding. The requirement for two consecutive contacts ensured the vehicle was generating sufficient energy to support recovery efforts. As the team had no telemetry to inform the current power state of the vehicle, contacts and their properties would be used to infer the power state.

Note: There are several reasons the vehicle may not respond the following day after a contact. Should the window end prematurely (i.e., < 30 minutes), the vehicle likely reached a low-power state and fault protection shut the vehicle down to prevent damage to the batteries. Other possible causes include the vehicle having insufficient power to support the window, missing an alarm clock due to environmental conditions, or tripping MCLK response.

Should MCLK be the running fault mode, the problem becomes further complicated. This is due to the fact that MCLK fault windows are much more challenging to predict. Unlike LFP and Uploss windows which execute at approximately 11:30 GST every Sol, MCLK windows could occur every Sol, every two Sols, every three Sols, twice in a single Sol, or may never execute. This is due to an adverse interaction between Deep Sleep, the hardcoded MCLK fault response, and when *Opportunity's* MCLK was reseeded.

7.4.2 Recovery Strategy

The MER Recovery Strategy consisted of the steps and processes to bring the rover back to nominal spacecraft (SCM) and communication (CBM) modes. Following fault mode determination and window characterization, the team conducts a data-gathering phase to fully assess the state of the rover and health of the subsystems. To ensure efficient use of each autonomous window, the team would command a High-Priority Communication Window, which executes immediately upon receipt, with increased uplink and downlink rates. Pieces of information the team requires include:

- Spacecraft Clock (SCLK): Required to recover clock to ephemeris time if in MCLK fault and determination of SCLK-SCET drift
- Recovery Time: Time stored in NVPM (Non-Volatile Parameter Module) which spacecraft uses if the MCLK register loses power; Solar-Array Wakeup (SAW) events to help predict next successive wakeups
- Active Fault Characterization: Confirms expected fault(s) from listening campaign from channelized telemetry
- BCB History: Provides important power and temperature telemetry from awake and asleep (CPU off) periods, including data on array current, battery voltage and battery temperature.
- Thermal Survey: Determines if thermal state satisfactorily characterized and Frequency Reference Offset (FRO) and Best-Lock Frequency (BLF) are sufficient for recovery

After sufficient data is gathered from the vehicle to characterize its state for recovery, the team holds a Go/No-Go review to determine:

1. Onboard fault modes and spacecraft state are fully understood
2. Sufficient information gathered to build recovery sequences for clearing running faults

3. Sufficient DSN coverage requested and available to proceed with recovery commanding
4. Team satisfied recovery can be undertaken safely and no additional risk exists to trip additional faults or re-enter existing faults

Depending on the type of active fault, the data-gathering process could take several days or several weeks. The recovery process itself is highly dependent on the active fault mode(s). For instance, for LPF only, the associated LPF monitors are cleared, the system-fault response stopped, and SCM and CBM modes transitioned to NOMINAL. For Uploss in addition to LPF, the uplink-loss timer is reset, the associated Uploss and LPF monitors cleared, the system-fault response stopped, and SCM and CBM modes transitioned to NOMINAL. MCLK response requires even more actions: 1) set the MCLK to "true" UTC, 2) reset the uplink-loss timer, 3) clear associated MCLK, Uploss, and LPF monitors, 4) stop the system fault response, and 5) transition SCM and CBM to NOMINAL mode.

During formulation of the recovery strategy, particular emphasis was placed on the order in which to clears all fault modes. For instance, MCLK fault is cleared first while Uploss and LPF are cleared on a subsequent uplink; this was considered after all onboard windows expired which, if all fault modes were cleared at once, would shut the vehicle down for 36 hours, only to wake up again without windows and shutting down again. The gap between clearing MCLK fault and Uploss/LPF allowed an *Opportunity* to load new windows.

7.4.3 Re-commissioning strategy

The MER recommissioning strategy consisted of the actions required to return the spacecraft to nominal science operations. The steps in the recommissioning effort ensured spacecraft systems and instruments were checked out in a logical and chronological order to prevent unnecessary degradation of hardware (i.e., excessive dust accumulation on the solar arrays or camera lenses, mobility actuators perform as expected prior to driving, etc.). The steps in the recommissioning effort included:

1. Establish Sequence Control
2. Pancam Mast Assembly (PMA) Calibration: Required for precise pointing of the PMA mast for PANCAM/NAVCAM imaging. PANCAMs used for multispectral imaging of science targets and Tau imaging, which is continuously trended during the recommissioning effort. NAVCAMs used for generating terrain maps for driving.
3. HGA Calibration: Required to use the HGA during X-band communications
4. Subsystem Checkouts: Continuous trending of subsystem health and performance
    - Power: Battery SOC, derived dust factor, and IDD heater On/Off periods
    - Thermal: PRT functionality, WEB thermal trending, heater checkouts (PANCAM electronics & filter wheels, mobility)
    - Telecommunications: SDST health checks, HGA pointing data, CE505 health checks
5. Communication Windows Loaded: Required as only a minimum number of X-band/UHF windows were loaded following transition to nominal spacecraft and communications modes.

Only after all above actions are completed satisfactorily is the rover declared healthy and usable for science.

7.4.4 Ground-based testing

The MER system testbeds were utilized to investigate system fault behaviors in dust storm power conditions and validate the fault recovery commanding strategies. The Cruise and EDL Testbed (CETB) was used to fully characterize the Low Power, Uploss, and MCLK faults and their interaction with Deep Sleep functionality. CETB was the highest fidelity venue for system fault testing, and included a battery simulator. One limitation of CETB was a faulty SDST simulator that triggered fault responses for bad 1553 bus transactions. However, the system response behavior was determined to be masked in Low Power, Uploss, and MCLK fault conditions. The Surface System Testbed (SSTB) was used to test the blind MCLK fault recovery sequences generated during each tactical planning shift. Sample sequences from each tactical plan were tested in the expected fault conditions for both MCLK and Uploss fault scenarios prior to radiating the sequences to the spacecraft. A sequencing error was caught by the SSTB testing in time for the file load to be corrected and uplinked.

7.5 Commanding strategies and operations

The formulated commanding strategies used by the recovery team were implemented by addressing highest-likelihood cases first (i.e., spacecraft did not POR from Deep-Sleep and is not running a fault response), corresponding to lowest overall commanding risk, to lowest-likelihood cases last (i.e., spacecraft trapped in MCLK "checkmate" scenario with very small Solar-Groovy window), corresponding to highest commanding risk. Commanding activities were requested based on the most likely time of Sol on Mars when *Opportunity* might be awake, made on a best effort's basis with the highly-taxed Deep Space Network array of communications dishes. The commanding strategies employed, in order, were:

1. Single "Beep" command radiated per day
2. "Sweep and Beep" Commanding
3. Left-Hand Circular (LCP) "Sweep and Beep" Commanding
4. Redundant Solid-State Amplifier Commanding
5. Blind MCLK Correction Commanding

7.5.1 Initial "beep" strategy

In the early days of the *Opportunity* recovery effort, a single command activate of the onboard "beep" sequence was sent to the rover at approximately 11:30 GST, which corresponded to the start of the autonomous fault window created by both LPF and Uploss fault. The intent of this strategy, should if have proved successful, was to both establish contact with the vehicle and power it down early to conserve onboard power. As these were the more likely executing fault states, they were employed until September 11th, when the team transitioned to a more complex commanding strategy to address a corner case for MCLK fault.

7.5.2 "Sweep and beep" strategy

The "Sweep and Beep" strategy was employed after several months of unsuccessful commanding with "beeps" around the expected Uploss fault window. Prior to implementation of this new strategy, the team identified a potentially fatal corner case with MCLK fault, creating a scenario where the vehicle would never autonomously respond, rendering the passive VSR technique useless. This scenario became known as a "checkmate" scenario, called such because utilizing only a passive listening technique would result in never hearing from the vehicle, even

if it had sufficient power to communicate and was listening for commands. In essence, the only

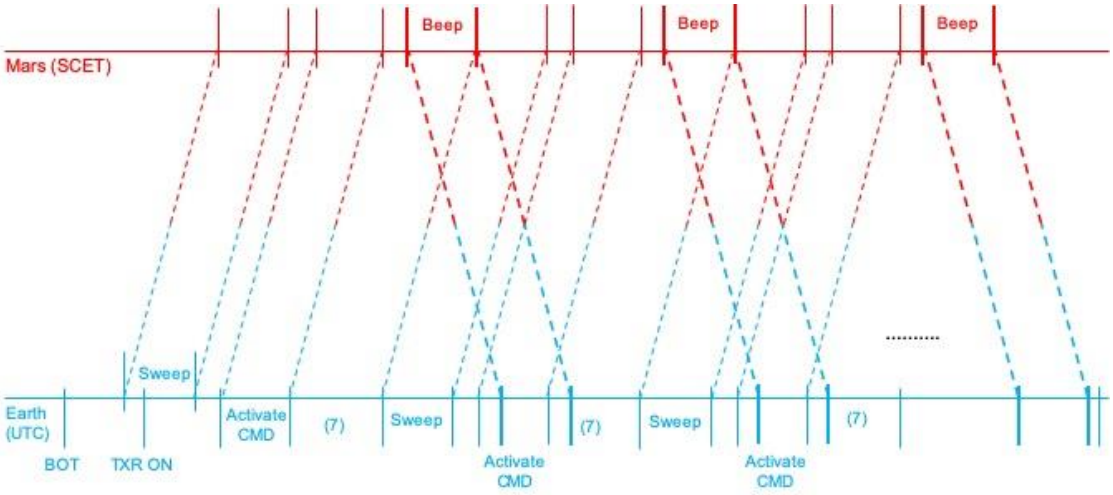

Fig. 7.5 Sweep and beep commanding strategy

method to elicit a response from the vehicle is through active commanding.

In a "Sweep and Beep" strategy, as the name implies, multiple acquisition sweeps and activates of *Opportunity's* onboard beep sequence are performed in a commanding session, as opposed to a single instance as was performed previously. With the addition of the temporal variable due to the unknown execution of MCLK fault windows, the search space expanded to account for the entire Solar-Groovy window, based on current best estimates of Tau and dust-factor. Within this space, a "Sweep and Beep" pair are spaced such that activates of beep sequences don't interfere with each other while providing sufficient margin for ground operators to search the recording bandwidth for the faint signal transmitted by the spacecraft in real-time. An overview of the technique is shown below in Figure 7.5.

In the diagram, actions by ground operators are represented in Blue and correspond to the DSN interface (Earth). Actions by *Opportunity*, if awake to receive commands, are represented in Red and correspond to the spacecraft interface (Mars). At first glance, the "Sweep and Beep" strategy is extremely busy, with a number of actions taking place in parallel, requiring precise and coordinated actions by the *Opportunity* Mission ACE, and DSN operator. Indeed, a learning curve occurred in the early days of executing the strategy while those involved became accustomed to the commanding sequence. In the early implementation of the strategy, margin was placed at the end of the expected "beep" window, prior to start of the next sequence activate, to allow the *Opportunity* Mission ACE to search for a possible signal. As the Earth-Mars distance increased, the strategy was modified to forgo real-time searches for in favor of performing more searches, relying on the VSR receivers to solely to detect "beep" signals from *Opportunity*. As the "Sweep and Beep" strategy probes the temporal region in the MCLK fault window search space.

7.5.2.1 MCLK "Checkmate" scenarios

A "Checkmate" scenario is defined as any scenario in MCLK fault in which a fault window NEVER executes. A "Checkmate" scenario occurs when either:

1. Following first boot after restoring power to the MCLK, the delta between "perceived" LST by the spacecraft and "true" LST is such that it prevents an autonomous fault window from executing due to an adverse interaction between MCLK fault behavior, deep-sleep behavior, and alarm clock behavior.
2. Due to poor environmental conditions (Tau + dust factor), the spacecraft generates insufficient Solar Array energy to support an autonomous fault window or possesses a relatively small Solar Groovy window which prevents execution of an autonomous fault window.

The implications from this observation are startling. First, it shows that only active commanding can elicit a responds from *Opportunity*; a passive, listening-only posture using the VSR is insufficient. And, second, recovery of the spacecraft is only possible by commanding into the background fault rate when the S/C is awake (solar-groovy window < 46 minutes in "Checkmate" scenario). Clearly, the scope of commanding had to be updated to address this corner case in the fault behavior; otherwise, continuing with the current commanding strategy would most certainly reduce the project's chances of making contact with the vehicle.

7.5.2.2 Simulated MCLK "Checkmate scenarios"

Deep Sleep behavior is a functionality that was implemented after landing, in response to an Instrument Deployment Device (IDD) joint heater being stuck in the enabled state. IDD heater power has been anomalously stuck in the enabled state since landing, such that the thermostat causes the heater to draw power whenever temperatures are sufficiently cold. Deep Sleep is a FSW functionality that causes the rover to disable battery discharging at 18:30 GST each night, disabling power to the system and preventing the IDD heaters from drawing energy during the colder overnight hours. When the rover bus voltage is raised sufficiently by the sunrise the following morning, the RPDU comes back online and re-enables battery discharging. This nominal Deep Sleep behavior is present in Low Power and Uploss Faults.

In the event of a MCLK fault, the rover enters a cycle of waking every 4 Mars-hours, searching for a time with sufficient solar array current to support DTE communications. However, if the rover wakes up after what it perceives as 18:30 GST, the subsequent shutdown disables battery discharging, with the following scheduled wakeup occurring with the batteries offline. When the alarm expires with the battery offline, the flight computer does not power on and the alarm clock snoozes to 27 Earth-hours. Sunrise reenables battery discharging the following morning, with the rover remaining powered down until the 27 Earth-hour alarm expires. Battery discharging remains enabled through the following night (as the alarm clock expired) with the IDD heater drawing power and draining the batteries. Note a Solar Array Wakeup (SAW) triggers the flight computer to power on when 2.0 Amps of current is generated by the solar panels, (only possible when skies were clear and solar panel array sufficiently clean.)

The Deep Sleep interaction with the MCLK fault created wakeup/shutdown cycles that reached a steady-state behavior with significant power consumption, as shown in Figure 7.6. A simulation tool was created to explore this steady-state behavior and determine possible progressions the rover could be placed into. The variables for this simulation included the initial time of Sol the MCLK reseeded with the recovery time (determines the actual solar time the rover perceived as 18:30 GST), the time of Sol where solar array power production was

sufficient to support DTE communication (a.k.a. Solar Groovy times), and when RPDU battery discharge control was reenabled. Initial MCLK seed times were varied in 5-minute increments over a 24-hour period, and Solar Groovy time ranges were varied from 1.5 to 4 hours in 30-minute increments.

The MCLK Fault simulations revealed that the rover can fall into wakeup progressions that supported communication windows twice per sol, once per sol, every other sol, every third sol, only once, or never (MCLK "Checkmate" Scenario, shown in Figure 7.7). The most commonly observed steady-state behaviors were one comm window every two sols and no comm windows supported. Additionally, the rover could fall into a configuration that only supports listening for communication on either RCP or LCP, without alternating polarizations. The simulations also revealed that Deep Sleep may only partially occur every other night, with some scenarios yielding no Deep Sleep at all. The lack of Deep Sleep would likely cause the rover to brown-out and pull the batteries offline within a few sols. This power-intensive fault behavior contributed to the urgency for recovering the vehicle before the arrival of Martian winter.

7.5.3 LCP "Sweep and beep" strategy

Although low in likelihood, a non-zero chance existed where *Opportunity* could be trapped in a "Checkmate" scenario on LCP polarization. In this scenario, the spacecraft executed an autonomous fault window at RCP polarization that went undetected by the ground (i.e., no VSR coverage at time of transmission or vehicle tripped LPF response at beginning of window); on subsequent wakeups, the criteria which creates a "Checkmate" scenario prevents the vehicle from autonomously responding at LCP.

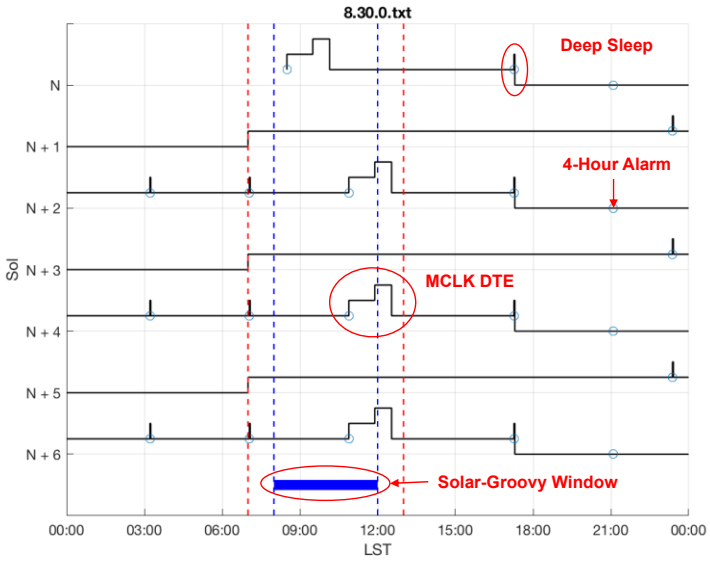

Fig. 7.6 Simulated MCLK fault behavior

As previously mentioned, MER's telecommunications design requires both uplink and downlink polarizations to match. As the vehicle is trapped in a LCP "Checkmate" scenario, a "Sweep and Beep" commanding strategy must be employed to elicit a response from the vehicle using acquisition sweeps and commands with LCP polarization; failure to do so would render all current "Sweep and Beep" commanding attempts useless as the onboard "beep" sequence utilized by the current strategy transmits at RCP polarization (i.e., the vehicle is also listening for commands at RCP). For this new modification to the current strategy, a new command was built which mimicked a "beep" at LCP polarization. While this was a trivial task, it increased the spacing between commanding attempts as sequenced commands contains more information than activates – the new command took twice as long to radiate as the previously used activate at

Opportunity's fault rate of 10 bps. It should be noted that by attempting LCP commanding, there was a small risk of permanently isolating *Opportunity's* HGA for the remainder of the mission should the spacecraft be recovered. As shown in Figure X, Coax Switch 1 (CXS-1) connects the LGA and HGA paths along the nominal RCP path; however, when executing a LCP fault window for the first time, CXS-1 actuates between to the LCP patch, enabling access to the LGA. Should this switch fail to actuate back to the original position following recovery, the spacecraft's HGA path would become permanently isolated, increasing operational complexity by needing to command at a much lower rate into the LGA.

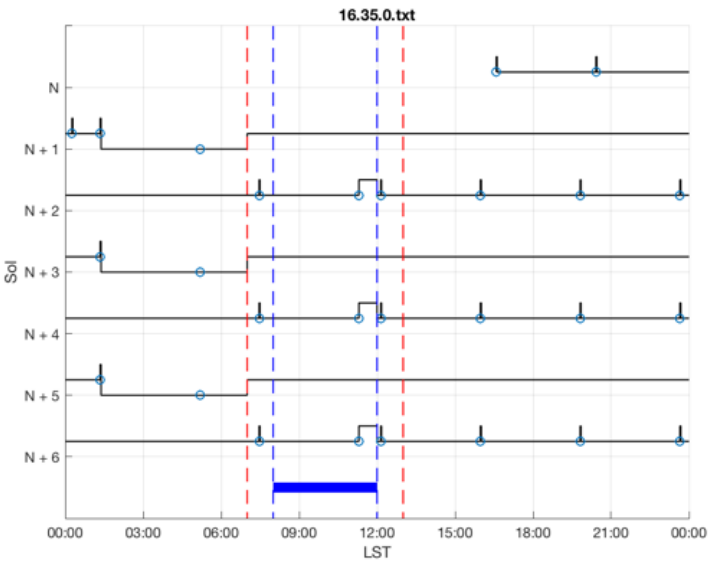

Fig. 7.7 MCLK "Checkmate" scenario

Following the addition of the LCP "Sweep and Beep" strategy, the team alternated between RCP and LCP commanding attempts, ensuring a minimum of three (3) successive attempts were made between polarization swaps (to account for the possibility of the vehicle waking up every three days in a "Checkmate" scenario).

7.5.4 "Hail Mary" Commanding strategy

"Hail Mary" commanding was to address low-likelihood, multiple-fault scenarios. These type of high-risk commanding scenarios were considered applicable only when current commanding efforts continued to yield no results and the project was approaching the end of the available recovery period. "Hail Mary" commanding scenarios addressed failures of both telecommunication system hardware (failure of primary or primary & redundant SSPAs) and continued unfavorable environmental conditions.

7.5.4.1 Redundant SSPA commanding strategy

All previous commanding assumed responses from the primary SSPA unit (SSPA-A). A lack of response to date suggested the prime SSPA unit may have failed. As with LCP "Sweep and Beep" commanding, continued commanding efforts using only the primary SSPA unit would continue to yield negative results if the hardware failed; as such, the team modified the "Sweep and Beep" strategy to include commands to exercise the redundant SSPA (SSPA-B) hardware. This modification increased commanding risk as the redundant SSPA had never been exercised in flight and required a violation of JPL flight practices (i.e., spacecraft shall not swap to redundant hardware if hardware on the current string is healthy). As *Opportunity* had failed to respond to any commanding to date, the team believed they had a compelling argument to exercise the backup hardware.

7.5.4.2 Blind MCLK commanding strategy

As the name implies, the blind MCLK commanding strategy involved correction of *Opportunity's* suspected out-of-sync MCLK to "true" SCLK in the blind (i.e., without real-time confirmation of the fault), clearing the active MCLK fault response, and transitioning the vehicle to Uploss fault. Recall that MCLK fault isolates the UHF communications path; if both SSPA units are suspected to have failed, then the only possibility to hear from *Opportunity* is through the UHF path. This strategy, considered last in the recovery efforts, was applicable for two (2) scenarios:

1. Poor atmospheric conditions, coupled with a significant layer of opaque dust on the Solar Arrays, results in a short Solar Groovy window, lower-energy production per Sol, and poor battery SOC (i.e., *Opportunity* doesn't have sufficient energy to autonomously respond)
2. Both SSPA units have failed

The symptoms for either scenario are the same: no contact from *Opportunity* despite "Sweep and Beep" commanding exercising RCP/LCP polarizations and prime/redundant SSPA units. As described in the beginning of this section, *Opportunity* had a limited window in which recovery of the vehicle was possible before permanent hardware damage from declining overnight temperatures set in. Unlike previous commanding strategies, unique recovery sequences were required for each commanding attempt as the MCLK was corrected to "true" SCLK each time; as the commanding was performed in the blind, the team required the MCLK to be as close to "true" SCLK as possible for accurate timing of Uploss fault windows and synchronization of deep-sleep to help the spacecraft's batteries begin to charge and enable consistent contacts beyond that point. In some cases, the spacecraft would transmit a "beep" after correcting the MCLK and clearing the fault; in others, a UHF window was included with the recovery commands and, following a requested shutdown of the vehicle, would wake up and respond to an orbiter hail, thus providing immediate confirmation success.

In total, 338 unique sequences, consisting of 20 individual commands, were built and sent to *Opportunity* in the span of one week. 682 sequences (with only a single command) were sent the previous seven months.

7.6 Why the vehicle was not recovered

The flight team will never really know when or how *Opportunity* was lost. We can, however, make some evidence-based conjecture based on data received in the last week of contact with the spacecraft. A likely failure mode was capacitance degradation and permanent damage to the batteries. Perhaps within a few days following loss of contact, a combination of cooler temperatures, lack of sufficient solar energy generation, and a parasitic load from the Mission Clock FPGA circuit led to irreparable, permanent damage to the cells. Trending the minimum SOC measurements from the final week, *Opportunity* may have had as much as eight (8) Sols or as few as four (4) Sols from last contact before cell damage began to occur. Another contributing factor was simply the shear amount and particle size of the lofted dust by the PEDE storm. MARCI-observed Tau measurements from the *Mars Reconnaissance Orbiter* indicated a highly-elevated dust environment (Tau > 3.0) over Perseverance Valley for months (estimated from early June through mid/late August). In parallel, lofted dust from the active lifting stage of the storm eventually fell back to the surface, which means *Opportunity* likely had a significant

accumulation of dust on its Solar Arrays. Due to the design of MER's power system, the lack of a under voltage-lockout (UVLO) circuit between the batteries and Mission-Clock FPGA circuit would allow a small parasitic charge to flow from the batteries, even with the clock powered down. Eventually, this load would drain the batteries to the point of damage. Finally, the Martian environment itself was a contributing factor, with several late-summer regional storms passing over Perseverance Valley during critical "Hail Mary" commanding activities. Unfortunately, there were too many adverse contributing factors for *Opportunity* to survive the 2018 PEDE storm, despite the best efforts of the recovery team.

8 References

Arvidson, R.E., et al. 2006, Nature and origin of the hematite-bearing plains of Terra Meridiani based on analyses of orbital and Mars Exploration rover data sets. *Journal of Geophysical Research: Planets, 111*(E12). doi: 10.1029/2006JE002728

Arvidson, R. E., et al. 2014, Ancient Aqueous Environments at Endeavour Crater, Mars. *Science*, 343(6169), doi:10.1126/science.1248097.

Arvidson, R. E., et al. 2016, High concentrations of manganese and sulfur in deposits on Murray Ridge, Endeavour Crater, Mars, *Am. Miner.*, 101(6), 1389-1405, DOI: 10.2138/am-2016-5599.

Ashley, J.W., et al., 2011, Evidence for mechanical and chemical alteration of iron-nickle meteorites on Mars: Process insights for Meridiani Planum. Journal of Geophysical Research 116:E00F20, doi: 10.1029/2010JE003672.

Beer, A.R., et al.. 2019. Bedrock Gully Erosion by Rockfall. *9th International Conference on Mars*, abs. no. 6431.

Chappelow, J. E. and Golombek, M.P. 2010, Event and conditions that produced the iron meteorite Block Island on Mars. *Journal of Geophysical Research: Planets, 115*(E7). doi: 10.1029/2006JE002728

Christensen, P.R. et al. 2001, Global mapping of Martian hematite mineral deposits: Remnants of water-driven processes on early Mars. *Journal of Geophysical Research: Planets, 106(E10).* doi: 10.1029/2000JE001415.

Clark, B.C., et al., 2016. Esperance: Multiple Episodes of Aqueous Alteration Involving Fracture Fills and Coatings at Matijevic Hill, Mars. *American Mineralogist*, 101, doi: 10.2138/am-2016-5575.

Crumpler, L.S. et al., 2015. Context of Ancient Aqueous Environments on Mars from in situ Geologic Mapping at Endeavour Crater. March. *JGR-Planets* 120, 538-569, doi: 10.1002/2014JE004699.

Crumpler, L.S. et al., 2018. First field examination of the near-surface rim structure on a large impact crater, *Opportunity* Rover, Endeavour Crater, Mars. Geological Society of America Abstracts with Programs, 50(6), Abstract #318088, doi:10.1130/abs/2018AM-318088.

Fenton, L.K., Carson, H.C., and Michaels, T.I. 2018, Climate Forcing of Ripple Migration and Crest Alignment in the Last 400 kyr in Meridiani Planum, Mars, *JGR Planets*, 123(4). doi: 10.1002/2017JE005503

Fox, V.K.,, et al., 2016. Smectite deposits in Marathon Valley, Endeavour Crater, Mars, identified using CRISM hyperspectral reflectance data. Geophysical Research Letters, 43, 4885-4892. doi: 10.1002/2016GL069108.

Golombek, M. et al., 2010. Constraints on ripple migration at Meridiani Planum from *Opportunity* and HiRISE observations of fresh craters, *JGR Planets*, 115 (E7). doi: 10.1029/2010JE003628

Golombek, M. et al., 2014. Erosion Rates and Mars Climate. Abstract for the 8th International Conference on Mars. July 14-18,

Golombek, M. et al., 2006. Erosion Rates at the Mars Exploration Rover Landing Sites and Long-term Climate Change on Mars. *JGR Planets*, 111(E12). doi: 10.1029/2006JE002754

Grant, J. A. et al., 2006. Crater Degradation in Gusev Crater and Meridiani Planum, Mars. *JGR Planets*: 111(E2). doi: 10.1029/2005JE002465

Grant, John A. et al., 2008. Degradation of Victoria Crater, Mars. *JGR Planets.* doi : 10.1029/2008JE003155

Grant, John A. et al., 2016. The Degradational History of Endeavour Crater, Mars. Icarus 280, 22–36

Grotzinger, J. et al., 2006, Sedimentary textures formed by aqueous processes, Erebus crater, Meridiani Planum, Mars. *Geology*, 34; 1085-1088 doi: 10.1130/G22985A.1.

Hughes et al., 2019, Degredation of Endeavour Crater based on orbital and rover-based observations in combination with landscape evolution modeling. *JGR: Planets*, 124, 6.

Hurowitz, Joel A. et al., 2010. Origin of acidic surface waters and the evolution of atmospheric chemistry on early Mars. Nature Geoscience, doi: 10.1038/NGEO831.

Lemmon, Mark et al, 2015. Dust aerosol, clouds, and the atmospheric optical depth record over 5 Mars years of the Mars Exploration Rover mission, *Icarus* 251, 96-111.

McLennan, S.M. et al., 2005. Provenance and Diagenesis of the Burns Formation, Meridiani Planum, Mars, *EPSL*, 240, 1.

Mittlefehldt, David W. et al.,2018, Diverse Lithologies and Alteration Events on the Rim of Noachian-Aged Endeavour Crater, Meridiani Planum, Mars: In-Situ Compositional Evidence. JGR-Planets; doi:10.1002/2017JE005474

Schröder, C. et al.,2016, Amazonian chemical weathering rate derived from stony meteorite finds at Meridiani Planum on Mars. Nature Communications 7, doi: 10.1038/ncomms13459.

Shirley, James H., 2015, Solar System dynamics and global-scale dust storms on Mars , *Icarus* 251, 128-144.

Stella, P and Herman, J. 2010. The Mars Surface Environment and Solar Array Performance , *35th IEEE Photovoltaic Specialists Conference*.

Sprague et al., 2012, Interannual similarity and variation in seasonal circulation of Mars' atmospheric Ar as seen by the gamma ray spectrometer on Mars Odyssey. *JGR: Planets*, 117, E4.

Squyres, S.W. et al., 2003, The Athena Mars Rover Science Investigation. *J. Geophys. Res.,* 108 (E12), 8062, doi:10.1029/2003JE002121.

Squyres, S.W. & Knoll, A.H. 2005. Sedimentary rocks at Meridiani Planum: Origin, diagenesis, and implications for life on Mars. *EPSL*¸ 240, 1.

Squyres, S.W. et al., 2012, Ancient Impact and Aqueous Processes at Endeavour Crater, Mars. Science 336, 570 doi: 10.1126/science.1220476.

Sullivan et al., 2019, MER *Opportunity* at Perseverance Valley: Evaluation of multiple working hypotheses for valley formation. LPSC 2019, abstract #3244.

VanBommel, S.J., Gellert, R., Clark, B.C., and Ming, D.W., 2018, Seasonal atmospheric Argon variability measured in the equatorial region of Mars by the Mars Exploration Rover Alpha Particle X-Ray Spectrometers: Evidence for an annual Argon-enriched front. JGR-Planets, 123(2), 544-558, doi:10.1002/2017JE005454.

Zurek, Richard, 1982, Martian Great Dust Storms: An Update , *Icarus* 50, 288-310.

9 Appendix: Team Publications List

9.1 Spirit Publications

Total Spirit papers: 77

JGR 2006: (20 papers)

- Arvidson: Overview of the Spirit Mars Exploration Rover Mission to Gusev Crater: Landing site to Backstay Rock in the Columbia Hills
- Cabrol: Aqueous processes at Gusev crater inferred from physical properties of rocks and soils along the Spirit traverse
- Clark: Evidence for montmorillonite or its compositional equivalent in Columbia Hills, Mars
- Farrand: Spectral variability among rocks in visible and near-infrared multispectral Pancam data collected at Gusev crater: Examinations using spectral mixture analysis and related techniques
- Gellert: Alpha Particle X-Ray Spectrometer (APXS): Results from Gusev crater and calibration report
- Golombek: Geology of the Gusev cratered plains from the Spirit rover transverse
- Greeley: Active dust devils in Gusev crater, Mars: Observations from the Mars Exploration Rover Spirit
- Greeley: Gusev crater: Wind-related features and processes observed by the Mars Exploration Rover Spirit
- Herkenhoff: Overview of the Microscopic Imager Investigation during Spirit's first 450 sols in Gusev crater
- Hurowitz: Mixing relationships and the effects of secondary alteration in the Wishstone and Watchtower Classes of Husband Hill, Gusev Crater, Mars
- Johnson: Spectrophotometric properties of materials observed by Pancam on the Mars Exploration Rovers: 1. Spirit
- Li: Spirit rover localization and topographic mapping at the landing site of Gusev crater, Mars
- McSween: Alkaline volcanic rocks from the Columbia Hills, Gusev crater, Mars
- McSween: Characterization and petrologic interpretation of olivine-rich basalts at Gusev Crater, Mars
- Ming: Geochemical and mineralogical indicators for aqueous processes in the Columbia Hills of Gusev crater, Mars
- Morris: Mössbauer mineralogy of rock, soil, and dust at Gusev crater, Mars: Spirit's journey through weakly altered olivine basalt on the plains and pervasively altered basalt in the Columbia Hills
- Ruff: The rocks of Gusev Crater as viewed by the Mini-TES instrument
- Squyres: Rocks of the Columbia Hills
- Wang: Evidence of phyllosilicates in Wooly Patch, an altered rock encountered at West Spur, Columbia Hills, by the Spirit rover in Gusev crater, Mars

- Wang: Sulfate deposition in subsurface regolith in Gusev crater, Mars

JGR 2008: (18 papers)

- Arvidson: Spirit Mars Rover Mission to the Columbia Hills, Gusev Crater: Mission overview and selected results from the Cumberland Ridge to Home Plate
- Cabrol: Soil sedimentology at Gusev Crater from Columbia Memorial Station to Winter Haven
- Campbell: Quantitative in situ determination of hydration of bright high-sulfate Martian soils
- Farrand: Rock spectral classes observed by the Spirit Rover's Pancam on the Gusev Crater Plains and in the Columbia Hills
- Fleischer: Depth selective Mössbauer spectroscopy: Analysis and simulation of 6.4 keV and 14.4 keV spectra obtained from rocks at Gusev Crater, Mars, and layered laboratory samples
- Greeley: Columbia Hills, Mars: Eolian features seen from the ground and orbit
- Lewis: Structure and stratigraphy of Home Plate from the Spirit Mars Exploration Rover
- Li: Characterization of traverse slippage experienced by Spirit rover on Husband Hill at Gusev crater
- McCoy: Structure, stratigraphy, and origin of Husband Hill, Columbia Hills, Gusev Crater, Mars
- McSween: Mineralogy of volcanic rocks in Gusev Crater, Mars: Reconciling Mössbauer, Alpha Particle X-Ray Spectrometer, and Miniature Thermal Emission Spectrometer spectra
- Ming: Geochemical properties of rocks and soils in Gusev Crater, Mars: Results of the Alpha Particle X-Ray Spectrometer from Cumberland Ridge to Home Plate
- Morris: Iron mineralogy and aqueous alteration from Husband Hill through Home Plate at Gusev Crater, Mars: Results from the Mössbauer instrument on the Spirit Mars Exploration Rover
- Schmidt: Hydrothermal origin of halogens at Home Plate, Gusev Crater
- Sullivan: Wind-driven particle mobility on Mars: Insights from Mars Exploration Rover observations at "El Dorado" and surroundings at Gusev Crater
- Usui: Petrogenesis of high-phosphorous Wishstone Class rocks in Gusev Crater, Mars
- Wang: Light-toned salty soils and coexisting Si-rich species discovered by the Mars Exploration Rover Spirit in Columbia Hills
- Yen: Hydrothermal processes at Gusev Crater: An evaluation of Paso Robles class soils
- Yingst: Morphology and texture of particles along the Spirit rover traverse from sol 450 to sol 745

JGR 2011: (10 papers)

- Arvidson: Spirit Mars Rover Mission: Overview and selected results from the northern Home Plate Winter Haven to the side of Scamander crater
- Crumpler: Field reconnaissance geologic mapping of the Columbia Hills, Mars, based on

Mars Exploration Rover Spirit and MRO HiRISE observations

- Greeley: Gusev Crater, Mars: Observations of three dust devil seasons
- Karunatillake: Regional and grain size influences on the geochemistry of soil at Gusev crater, Mars
- Li: MER Spirit rover localization: Comparison of ground image– and orbital image–based methods and science applications
- McGlynn: Origin of basaltic soils at Gusev crater, Mars, by eolian modification of impact-generated sediment
- Rice: Temporal observations of bright soil exposures at Gusev crater, Mars
- Ruff: Characteristics, distribution, origin, and significance of opaline silica observed by the Spirit rover in Gusev crater, Mars
- Wang: Ferric sulfates on Mars: A combined mission data analysis of salty soils at Gusev crater and laboratory experimental investigations
- Yingst: Constraints on the geologic history of "Home Plate" materials provided by clast morphology and texture

Science 2004: (11 papers)

- Arvidson: Localization and Physical Properties Experiments Conducted by Spirit at Gusev Crater
- Bell: Pancam Multispectral Imaging Results from the Spirit Rover at Gusev Crater
- Bertelsen: Magnetic Properties Experiments on the Mars Exploration Rover Spirit at Gusev Crater
- Christensen: Initial Results from the Mini-TES Experiment in Gusev Crater from the Spirit Rover
- Gellert: Chemistry of Rocks and Soils in Gusev Crater from the Alpha Particle X-ray Spectrometer
- Grant: Surficial Deposits at Gusev Crater Along Spirit Rover Traverses
- Greeley: Wind-Related Processes Detected by the Spirit Rover at Gusev Crater, Mars
- Herkenhoff: Textures of the Soils and Rocks at Gusev Crater from Spirit's Microscopic Imager
- McSween: Basaltic Rocks Analyzed by the Spirit Rover in Gusev Crater
- Morris: Mineralogy at Gusev Crater from the Moessbauer Spectrometer on the Spirit Rover
- Squyres: The Spirit Rover's Athena Science Investigation at Gusev Crater, Mars

Additional: (18 papers)

- Cabrol: Sands at Gusev Crater, Mars. **(JGR-Planets 2014)**
- Crumpler: MER geologic traverse by the Spirit rover in the Plains of Gusev Crater, Mars (**Geology 2005**)
- Fleischer: Coatings and weathering rinds at Gusev crater, Mars, investigated by depth selective Mössbauer spectroscopy (**Hyperfine Interact 2008**)
- Grant: Distribution of rocks on the Gusev Plains and on Husband Hill, Mars (**Geophys**

Res. Ltrs 2006)

- Greeley: Fluid lava flows in Gusev crater, Mars (**JGR Vol. 110 2005**)
- Greeley: Martian variable features: New insight from the Mars Express Orbiter and the Mars Exploration Rover Spirit (**JGR Vol. 110 2005**)
- Hamilton: Distribution and characteristics of Adirondack-class basalt as observed by Mini-TES in Gusev crater, Mars and its possible volcanic source. (**Icarus 2012**)
- Haskin: Water alteration of rocks and soils on Mars at the Spirit rover site in Gusev crater (**Nature 2005**)
- Johnson: Mineralogic constraints on sulfur-rich soils from Pancam spectra at Gusev crater, Mars (**Geophys Res Ltrs 2007**)
- Li: Rigorous Photogrammetric Processing of HiRISE Stereo Imagery for Mars Topographic Mapping (**IEEE Transactions on Geoscience and Remote Sensing**)
- Lichtenberg: Coordinated analysis of orbital and Spirit rover data to characterize surface materials on the cratered plains of Gusev Crater, Mars (**JGR-Planets 2007**)
- Morris: Identification of carbonate-rich outcrops on Mars by the Spirit rover (**Science 2010**)
- Rice: Silica-rich deposits and hydrated minerals at Gusev Crater, Mars: Vis-NIR spectral characterization and regional mapping **(Icarus 2010)**
- Ruff: Evidence for a Noachian-Aged Ephemeral Lake in Gusev Crater, Mars. **(Geology 2014)**
- Schmidt: Spectral, mineralogical, and geochemical variations across Home Plate, Gusev crater, Mars indicate high and low temperature alteration (**EPSL 2009**)
- Squyres: Detection of silica-rich deposits on Mars (**Science 2008**)
- Squyres: Pyroclastic activity at Home Plate in Gusev crater, Mars (**Science 2007**)
- Vaughan: Pancam and Microscopic Imager observations of dust on the Spirit Rover: Cleaning events, spectral properties, and aggregates. (**Mars 2010**)

9.2 Two-Rover Publications

Total two rover papers: 74

Icarus: (5 papers)

- Johnson (2015): **Spectrophotometric properties of materials observed by Pancam on the Mars Exploration Rovers: 3. Sols 500-1525**.
- Lemmon (2014): Dust aerosol, clouds, and the atmospheric optical depth record over 5 Mars years of the Mars Exploration Rover mission.
- Spanovich (2006): Surface and near-surface atmospheric temperatures for the Mars Exploration Rover landing sites.
- Wang (2013): The preservation of subsurface sulfates with mid-to-high degree of hydration in equatorial regions on Mars.
- Wang and Zhou (2014): Experimental comparison of the pathways and rates of the dehydration of Al-, Fe-, Mg-, and Ca-sulfates under Mars relevant conditions.

JGR 2003: (13 papers)

- Arvidson: Physical properties and localization investigations associated with the 2003 Mars Exploration rovers
- Bell: Mars Exploration Rover Athena Panoramic Camera (Pancam) investigation
- Christensen: Miniature Thermal Emission Spectrometer for the Mars Exploration Rovers
- Crisp: Mars Exploration Rover mission
- Golombek: Rock size-frequency distributions on Mars and implications for Mars Exploration Rover landing safety and operations
- Golombek: Selection of the Mars Exploration Rover landing sites
- Gorevan: Rock Abrasion Tool: Mars Exploration Rover mission
- Herkenhoff: Athena Microscopic Imager investigation
- Klingelhöfer: Athena MIMOS II Mössbauer spectrometer investigation
- Madsen: Magnetic Properties Experiments on the Mars Exploration Rover mission
- Maki: The Mars Exploration Rover engineering cameras
- Rieder: The new Athena alpha particle X-ray spectrometer for the Mars Exploration Rovers
- Squyres: Athena Mars rover science investigation

JGR 2006: **(9 papers)**

- Bell: In-flight calibration and performance of the Mars Exploration Rover Panoramic Camera (Pancam) instruments
- Golombek: Erosion rates at the Mars Exploration Rover landing sites and long-term climate change on Mars
- Grant: Crater gradation in Gusev crater and Meridiani Planum, Mars
- Hurowitz: In situ and experimental evidence for acidic weathering of rocks and soils on Mars
- Johnson: Radiative transfer modeling of dust-coated Pancam calibration target materials: Laboratory visible/near-infrared spectrogoniometry
- Kinch: Dust deposition on the Mars Exploration Rover Panoramic Camera (Pancam) calibration targets
- Smith: One Martian year of atmospheric observations using MER Mini-TES
- Wolff: Constraints on dust aerosols from the Mars Exploration Rovers using MGS overflights and Mini-TES
- Yen: Nickel on Mars: Constraints on meteoritic material at the surface

JGR 2008: (7 papers)

- Arvidson: Introduction to special section on Results from the Mars Exploration Rover Spirit and *Opportunity* Missions
- Bell: Surface albedo observations at Gusev Crater and Meridiani Planum, Mars
- Goetz: Search for magnetic minerals in Martian rocks: Overview of the Rock Abrasion Tool (RAT) magnet investigation on Spirit and *Opportunity*
- Madsen: Overview of the magnetic properties experiments on the Mars Exploration Rovers

- Schröder: Meteorites on Mars observed with the Mars Exploration Rovers
- Soderblom: Mars Exploration Rover Navigation Camera in-flight calibration
- Treguier: Overview of Mars surface geochemical diversity through Alpha Particle X-Ray Spectrometer data multidimensional analysis: First attempt at modeling rock alteration

JGR 2011: (4 papers)

- Arvidson: Introduction to special section on Spirit and *Opportunity* Results
- Geissler: Gone with the wind: Eolian erasure of the Mars Rover tracks
- McSween: Determining the modal mineralogy of Martian soils
- Sullivan: Cohesions, friction angles, and other physical properties of Martian regolith from Mars Exploration Rover wheel trenches and wheel scuffs

Nature 2005: (4 papers)

- Bell: Solar eclipses of Phobos and Deimos observed from the surface of Mars
- Goetz: Indication of drier periods on Mars from the chemistry and mineralogy of atmospheric dust
- Golombek: Assessment of Mars Exploration Rover landing site predictions
- Yen: An integrated view of the chemistry and mineralogy of martian soils

Additional: (32 papers)

- Bell: Mars Exploration Rover Pancam multispectral imaging of rocks, soils, and dust at Gusev crater and Meridiani Planum (**chapter 13 of book The Martian Surface: Composition, Mineralogy, and Physical Properties, ed. J. F. Bell III 2008**)
- Brȍckner: Mars Exploration Rovers: chemical composition by the APXS (**chapter 4 of book The Martian Surface: Composition, Mineralogy, and Physical Properties, ed. J. F. Bell III 2008**)
- Goetz: Magnetic properties of Martian surface materials (**chapter 16 of book The Martian Surface: Composition, Mineralogy, and Physical Properties, ed. J. F. Bell III 2008**)
- Golombek: Mars: Landing Site Geology, Mineralogy and Geochemistry (**Encyclopedia of the Solar System 2007 by Academic Press**)
- Herkenhoff: In-situ observations of the physical properties of the Martian surface **(Ch. 20, The Martian Surface: Composition, Mineralogy, and Physical Properties, ed. J. F. Bell III 2008**)
- Hurowitz: A ~3.5 Ga record of water-limited, acidic weathering conditions on Mars (**EPSL 2007**)
- Johnson: **Discrete element method simulations of Mars Exploration Rover wheel performance. (Journal of Terramechanics 2015)**
- Karunatillake: Chemical compositions at Mars landing sites subject to Mars Odyssey Gamma Ray Spectrometer constraints (**JGR Vol. 112 2007**)
- Knoll: Water on Mars and the Prospect of Martian Life **(Elements 2006)**
- Knuth and Johnson: Discrete element modeling of a Mars Exploration Rover wheel in granular material **(Science Direct 2011)**

- Knuth: Discrete element modeling of a Mars Exploration Rover wheel in granular material. **(Journal of Terramechanics 2012)**
- Li: Rover Localization and Landing-Site Mapping Technology for the 2003 Mars Exploration Rover Mission (**Photogrammetric Engineering & Remote Sensing 2004**)
- Li: Initial Results of Rover Localization and Topographic Mapping for the 2003 Mars Exploration Rover Mission (**Photogrammetric Engineering & Remote Sensing 2005)**
- Li: Localization of Mars rovers using descent and surface-based image data (**JGR Vol 107 2002**)
- Liu and Wang: Dehydration of Na-jarosite, ferricopiapite, and rhomboclase at temperatures of 50 and 95 degrees C: implications for Martian ferric sulfates. **(Journal of Raman Spectroscopy 2015)**
- McGlynn: Soil mineralogy at the Mars Exploration Rover landing sites: An assessment of the competing roles of physical sorting and chemical weathering. (**JGR-Planets 2012**)
- McLennan: The sedimentary rock cycle of Mars (**chapter 24 of book The Martian Surface: Composition, Mineralogy, and Physical Properties, ed. J. F. Bell III, 2008)**
- McLennan: Sulfur on Mars (**Elements 2010**)
- McSween: Elemental Composition of the Martian Crust (**Science 2009**)
- Morris: Iron mineralogy and aqueous alteration on Mars from the MER Mössbauer spectrometers (**chapter 15 of book The Martian Surface: Composition, Mineralogy, and Physical Properties, ed. J. F. Bell III, 2008)**
- Ruff: The mineralogy of Gusev crater and Meridiani Planum derived from the Miniature Thermal Emission Spectrometers on the Spirit and *Opportunity* rovers (**Ch 14, The Martian Surface: Composition, Mineralogy, and Physical Properties, ed. J. F. Bell III, pp. 315-338, 2008)**
- Schröder: Weathering of Fe-bearing minerals under Martian conditions, investigated by Mössbauer spectroscopy (**Planetary and Space Science 2004**)
- Schröder: Mössbauer spectroscopy as a tool in astrobiology (**Hyperfine Interact 2006**)
- Schröder: Fe Mössbauer spectroscopy as a tool in astrobiology (**Planetary and Space Science 2006**)
- Schröder: Extraterrestrial Mössbauer spectroscopy: more than 3 years of Mars exploration and developments for future missions (**Hyperfine Interact 2008**)
- Schröder: Field-portable Mössbauer spectroscopy on Earth, the Moon, Mars, and beyond (**Geochemistry: Exploration, Environment, Analysis 2011**)
- Smith: First atmospheric science results from the Mars Exploration Rovers' Mini-TES (**Science 2004**)
- Tosca: Water Activity and the Challenge for Life on Early Mars (**Science 2008**)
- Tosca: Chemical divides and evaporite assemblages on Mars (**EPSL 2006**)
- Tosca: Juvenile chemical sediments and the long term persistence of water at the surface of Mars (**EPSL 2009)**
- Wang and Jolliff: Setting Constraints on the Nature and Origin of the Two Major Hydrous

Sulfates on Mars, Kieserite and Polyhydrated Sulfate. **(Accepted by JGR-Planets 2016)**

- Wilson: Pedogenic hematitic concretions from the Triassic New Haven Arkose, Connecticut: Implications for understanding Martian diagenetic processes. (**Chemical Geology 2012**)

9.3 *Opportunity* Publications

Total Opportunity papers: 64

JGR 2003: (2 papers)

- Arvidson: Mantled and exhumed terrains in Terra Meridiani, Mars
- Greeley: Mars: Eolian features and wind predictions at the Terra Meridiani and Isidis Planitia potential Mars Exploration Rover landing sites

JGR 2006: (11 papers)

- Arvidson: Nature and origin of the hematite-bearing plains of Terra Meridiani based on analyses of orbital and Mars Exploration rover data sets
- Bell: Chromaticity of the Martian sky as observed by the Mars Exploration Rover Pancam instruments
- Farrand: Visible and near-infrared multispectral analysis of rocks at Meridiani Planum, Mars, by the Mars Exploration Rover *Opportunity*
- Glotch: Determination and interpretation of surface and atmospheric Miniature Thermal Emission Spectrometer spectral end-members at the Meridiani Planum landing site
- Glotch: Mineralogy of the light-toned outcrop at Meridiani Planum as seen by the Miniature Thermal Emission Spectrometer and implications for its formation
- Goetz: Search for magnetic minerals in Martian rocks: Overview of the Rock Abrasion Tool (RAT) magnet investigation on Spirit and *Opportunity*
- Johnson: Spectrophotometric properties of materials observed by Pancam on the Mars Exploration Rovers: 2. *Opportunity*
- Li: *Opportunity* rover localization and topographic mapping at the landing site of Meridiani Planum, Mars
- Morris: Mössbauer mineralogy of rock, soil, and dust at Meridiani Planum, Mars: *Opportunity*'s journey across sulfate-rich outcrop, basaltic sand and dust, and hematite lag deposits
- Squyres: Overview of the *Opportunity* Mars Exploration Rover Mission to Meridiani Planum: Eagle Crater to Purgatory Ripple
- Weitz: Soil grain analyses at Meridiani Planum, Mars

JGR 2008: (5 papers)

- Calvin: Hematite spherules at Meridiani: Results from MI, Mini-TES, and Pancam
- Geissler: First in situ investigation of a dark wind streak on Mars
- Grant: Degradation of Victoria crater, Mars
- Herkenhoff: Surface processes recorded by rocks and soils on Meridiani Planum, Mars:

Microscopic Imager observations during *Opportunity*'s first three extended missions

- Knoll: Veneers, rinds, and fracture fills: Relatively late alteration of sedimentary rocks at Meridiani Planum, Mars

JGR 2011: (10 papers)

- Arvidson: *Opportunity* Mars Rover mission: Overview and selected results from Purgatory ripple to traverses to Endeavour crater
- Ashley: Evidence for mechanical and chemical alteration of iron-nickel meteorites on Mars: Process insights for Meridiani Planum
- Chappelow: Event and conditions that produced the iron meteorite Block Island on Mars
- Chojnacki: Orbital observations of contemporary dune activity in Endeavour crater, Meridiani Planum, Mars
- Fleischer: Distinct hematite populations from simultaneous fitting of Mössbauer spectra from Meridiani Planum, Mars
- Fleischer: Mineralogy and chemistry of cobbles at Meridiani Planum, Mars, investigated by the Mars Exploration Rover *Opportunity*
- Golombek: Constraints on ripple migration at Meridiani Planum from *Opportunity* and HiRISE observations of fresh craters
- Hayes: Reconstruction of eolian bed forms and paleocurrents from cross-bedded strata at Victoria Crater, Meridiani Planum, Mars
- Schröder: Properties and distribution of paired candidate stony meteorites at Meridiani Planum, Mars
- Weitz: Visible and near-infrared multispectral analysis of geochemically measured rock fragments at the *Opportunity* landing site in Meridiani Planum

JGR-Planets MER Special Section: (12 papers)

- Arvidson (2015): **Mars Reconnaissance Orbiter and *Opportunity* Observations of Burns Formation and Underlying Strata: Crater Hopping at Meridiani Planum.**
- Cabrol (2014): Sands at Gusev Crater, Mars.
- Clark (2014): Esperance: Multiple Episodes of Aqueous Alteration Involving Fracture Fills and Coatings at Matijevic Hill, Mars.
- Crumpler (2014): Mars Exploration Rover *Opportunity* In Situ Geologic Context of Phyllosilicate-bearing Outcrops, Cape York Rim Segment, Endeavour Crater.
- Crumpler (2015): **Context of Ancient Aqueous Environments on Mars from in situ Geologic Mapping at Endeavour Crater.**
- Farrand (2014): **Observations of rock spectral classes by the *Opportunity* rover's Pancam on northern Cape York and on Matijevic Hill, Endeavour Crater, Mars.**
- Geissler (2014): The birth and death of transverse eolian ridges on Mars.
- Golombek (2014): **Small crater modification on Meridiani Planum and implications for erosion rates and climate change on Mars**
- Herkenhoff (2014): Overview of Spirit Microscopic Imager Results.
- Parker (2014): Coastal geomorphology and stratigraphy at Endeavour Crater

- Ruff (2014): Wishstone to Watchtower: Alteration of plagioclase-rich rocks in Gusev crater, Mars.
- Schröder (2014): Possible association of ferrous phosphates and ferric sulfates in hydrothermal deposits in Gusev Crater, Mars.

Science 2004: (11 papers)

- Arvidson: Localization and Physical Property Experiments Conducted by *Opportunity* at Meridiani Plan
- Bell: Pancam Multispectral Imaging Results from the *Opportunity* Rover at Meridiani Planum
- Christensen: Mineralogy at Meridiani Planum from the Mini-TES Experiment on the *Opportunity* Rover
- Herkenhoff: Evidence from *Opportunity*'s Microscopic Imager for Water on Meridiani Planum
- Klingelhöfer: Jarosite and Hematite at Meridiani Planum from *Opportunity*'s Mössbauer Spectromete
- Lemmon: Atmospheric Imaging Results from the Mars Exploration Rovers: Spirit and *Opportunity*
- Rieder: Chemistry of Rocks and Soils at Meridiani Planum from the Alpha Particle X-ray Spectrometer
- Smith: First Atmospheric Science Results from the Mars Exploration Rovers Mini-TES
- Soderblom: Soils of Eagle Crater and Meridiani Planum at the *Opportunity* Rover Landing Site
- Squyres: In Situ Evidence for an Ancient Aqueous Environment at Meridiani Planum, Mars
- Squyres: The *Opportunity* Rover's Athena Science Investigation at Meridiani Planum, Mars

EPSL 2005: (7 papers)

- Clark: Chemistry and mineralogy of outcrops at Meridiani Planum
- Grotzinger: Stratigraphy and sedimentology of a dry to wet eolian depositional system, Burns formation, Meridiani Planum, Mars
- Knoll: An astrobiological perspective on Meridiani Planum
- McLennan: Provenance and diagenesis of the evaporite-bearing Burns formation, Meridiani Planum, Mars
- Morris: Hematite spherules in basaltic tephra altered under aqueous, acid-sulfate conditions on Mauna Kea volcano, Hawaii: Possible clues for the occurrence of hematite-rich spherules in the Burns formation at Meridiani Planum, Mars
- Squyres: Sedimentary rocks at Meridiani Planum: Origin, diagenesis, and implications for life on Mars
- Tosca: Geochemical modeling of evaporation processes on Mars: Insight from the sedimentary record at Meridiani Planum

Additional: (24 papers)

- Arvidson: Ancient Aqueous Environments at Endeavour Crater, Mars (**Science 2014**)
- Arvidson: High Concentrations of Manganese and Sulfur in Deposits on Murray Ridge, Endeavour Crater. **(American Mineralogist 2016)**
- Arvidson: **Manganese Enrichments in Endeavour Crater, Mars, and Implications for Past Aqueous Conditions. (Nature Geoscience 2014)**
- **Chojnacki: Persistant eolian activity at Endeavour crater, Meridiani Planum, Mars; new observations from orbit and the surface. (Icarus 2015)**
- **Clark: Esperance: Multiple Episodes of Aqueous Alteration Involving Fracture Fills and Coatings at Matijevic Hill, Mars. (American Mineralogist, accepted 2016)**
- Edgar: Stratigraphic Architecture of Bedrock Reference Section, Victoria Crater, Meridiani Planum, Mars. (**Sedimentary Geology of Mars SEPM Special Publication 2012**)
- Edgar: Hypotheses for the origin of fine-grained sedimentary rocks at Santa Maria crater. **(Icarus 2014)**
- Farrand: VNIR Multispectral Observations of Rocks at Cape York, Endeavour Crater, Mars by the *Opportunity* Rover's Pancam. (**Icarus 2013**)
- Fleischer: New insights into the mineralogy and weathering of the Meridiani Planum meteorite, Mars (**Meteoritics & Planetary Science 2011**)
- Fralick: Potential Recognition of Accretionary Lapilli in Distal Impact Deposits on Mars: A Facies Analog Provided by the 1.85 GA Sudbury Impact Deposit. (**Sedimentary Geology of Mars SEPM Special Publication 2012**).
- Gaines: Strategic analysis for the MER Cape Verde approach **(IEEE Aerospace 2009**)
- Grant: The Degradational History of Endeavour Crater. **(Submitted to Icarus 2015)**
- Grotzinger: Sedimentary textures formed by aqueous processes, Erebus crater, Meridiani Planum, Mars (**Geology 2006**)
- Hurowitz: Origin of acidic surface waters and the evolution of atmospheric chemistry on early Mars (**Nature Geoscience 2010**)
- Knoll: Exploration of Victoria Crater by the rover *Opportunity* (**Science 2009**)
- Metz: Sulfate-rich eolian and wet interdune deposits, Erebus crater, Meridiani Planum , Mars (**J. Sediment Res 2009)**
- Noe: Hydrated minerals on Endeavour Crater's rim and interior, and surrounding plains: New insights from CRISM data (**GRL 2012**)
- Ruecker: Geochemistry and mineralogy of Western Australian salt lake sediments and their potential as analogue for Meridiani Planum on Mars. **(Astrobiology 2016, in press)**
- Squyres: Ancient impact and aqueous processes at Endeavour Crater, Mars (**Science 2012**)
- Squyres: Two years at Meridiani Planum: Results from the *Opportunity* rover (**Science 2006**)
- Sullivan: Eolian processes at the Mars Exploration Rover Meridiani Planum landing site (**Nature 2005**)

- Szalai: Mars Exploration Rover Heatshield Observation Campaign (**42nd AIAA Thermophysics Conference**)
- Watters: Origin of the structure and planform of small impact craters in fractured targets: Endurance Crater at Meridiani Planum, Mars. (**Icarus 2011**)
- Zipfel: Bounce Rock – A shergottite-like basalt encountered at Meridiani Planum, Mars (**Meteoritics and Planetary Science 2011)**

GRAND TOTAL: 233 papers (as of 2016-04-08)